HYDROTHERMAL ALTERATION ASSOCIATED WITH MASSIVE SULFIDE DEPOSITS, MIDDLE VALLEY, NORTHERN JUAN DE FUCA RIDGE*

WAYNE D. GOODFELLOW, KATE GRAPES, BARRY CAMERON AND JIM M. FRANKLIN

Geological Survey of Canada, 601 Booth Street, Ottawa, Ontario K1A 0E8

ABSTRACT

Middle Valley is a sediment-covered rift near the northern extremity of the Juan de Fuca Ridge. Hydrothermal fluids are presently being discharged at two vent fields about 3 km apart, Bent Hill (BH) and the Area of Active Venting (AAV). At the AAV, the hydrothermal alteration consists of an inner, spatially restricted, higher-temperature (>120°C) zone (Zone I) that consists of grey, moderately to strongly indurated, and locally brecciated, fractured and veined sediment. Hydrothermal minerals within Zone I include a Mg-rich smectite-group mineral, chlorite, amorphous silica, barite, pyrite and gypsum. Zone I is surrounded by a more widespread, lower-temperature (<120°C) zone (Zone II) that consists of moderately indurated, blue-green sediments that consist of a Mg-rich smectite-group mineral, carbonate, barite and minor pyrite. The zonal distribution of hydrothermal minerals is controlled by the chemical and physical evolution of high-temperature (up to 274°C) fluid as it migrated outward and upward from a central conduit, reacted with detrital and biogenic minerals, and mixed with downwelling seawater. This model of fluid migration is supported by 1) heat flow values and temperatures based on oxygen isotope fractionation in hydrothermal minerals, which decrease away from vent sites, 2) $^{87}Sr/^{86}Sr$ ratios for hydrothermal minerals that define a mixing line, from less radiogenic hydrothermal Sr near the vent sites to more radiogenic Sr distal from vent sites; 3) $\delta^{13}C$ values in carbonate concretions that range from moderately negative (about −15‰) in Zone I to highly negative (−30‰) in Zone II; 4) $\delta^{34}S$ values in hydrothermal pyrite that are similarly zoned, from positive values (0.8 to 7.5‰) in Zone I to highly negative values (−14.3 to −39.7‰) in Zone II; 5) pore-water compositions that define a convex-upward hydrothermal acidic plume enriched in Ca, Si and Ba, and depleted in Mg; and 6) stratabound zones of alteration associated with highly permeable sediment that suggest an along-strata control on permeability.

Keywords: Juan de Fuca Ridge, Middle Valley, vents, hydrothermal alteration, mineralogy, geochemistry, isotopes.

SOMMAIRE

Middle Valley, zone d'extension recouverte de sédiments, se trouve près de l'extrémité nord de la crête de Juan de Fuca. Des phénomènes hydrothermaux y ont été repérés à deux centres d'activité, "Bent Hill" (BH) et "Area of Active Venting" (AAV), séparés par 3 km. Dans le centre AAV, l'altération hydrothermale se manifeste par une zone (dite "zone I") interne, restreinte, à température élevée (>120°C), dans laquelle les sédiments sont gris, plus ou moins endurcis, et localement bréchifiés, fissurés et recoupés par des veines. Parmi les minéraux de la zone I, nous trouvons un membre magnésien du groupe de la smectite, chlorite, silice amorphe, barite, pyrite et gypse. La zone I est entourée par la zone II, plus répandue, à température plus faible (<120°C), dans laquelle les sédiments, bleu-vert, sont moins fortement endurcis et contiennent un membre magnésien du groupe de la smectite, carbonate, barite et pyrite. La distribution des minéraux hydrothermaux en zones dépendrait de l'évolution physicochimique du fluide de haute température (jusqu'à 274°C) à mesure qu'il se propageait vers le haut et l'extérieur le long d'un conduit central, réagissant avec des matériaux détritiques et biogéniques, et se mélangeant avec l'eau de mer, plus dense. Ce modèle de migration de la phase fluide repose sur 1) les données de flux de chaleur et les températures indiquées par le fractionnement des isotopes d'oxygène dans les minéraux hydrothermaux, qui diminuent avec la distance à partir d'un évent, 2) le rapport $^{87}Sr/^{86}Sr$ des minéraux hydrothermaux, dont les valeurs définissent un mélange impliquant le Sr plus faiblement radiogénique près des évents et le Sr plus fortement radiogénique aux sites plus éloignés des évents, 3) le rapport $\delta^{13}C$ dans les concrétions carbonatées, dont les valeurs vont de modérément négatives (environ −15‰) dans la zone I à fortement négatives (−30‰) dans la zone II, 4) le rapport $\delta^{34}S$, dont les valeurs dans la pyrite hydrothermale aussi sont zonées, de positives (0.8 à 7.5‰) dans la zone I à fortement négatives (−14.3 à −39.7‰) dans la zone II, 5) la composition de l'eau des pores des sédiments, qui définit un panache hydrothermal convexe vers le haut, enrichi en Ca, Si et Ba, et appauvri en Mg, et 6) la présence de zones d'altération confinées en strates, associées avec des couches de sédiments dont la perméabilité aurait promu une circulation latérale, le long des strates.

(Traduit par la Rédaction)

Mots-clés: crête de Juan de Fuca, Middle Valley, évents, altération hydrothermale, minéralogie, géochimie, isotopes.

INTRODUCTION

Middle Valley, an oceanic rift at the northernmost part of the Juan de Fuca Ridge (Fig. 1), has been partly filled by interbedded hemipelagic and turbiditic sediments. Seismic profiles show that the sedimentary sequence thickens from a few meters near the margins of the rift to hundreds of meters near the center, and northward toward the Sovanco Transform, where thicknesses greater than 1000 m have been estimated (Davis & Villinger 1992). Two major areas of discharge of hydrothermal fluid and deposition of sulfides have been described within Middle Valley, Bent Hill (BH) and the Area of Active Venting (AAV) (Fig. 2; Davis et al. 1987, Goodfellow & Blaise 1988, Goodfellow & Franklin, in press).

This paper describes the mineralogy and geochemistry of unaltered and hydrothermally altered sediment cores collected in Middle Valley between 1985 and 1990. Most of the cores are from the BH (35 cores) and the AAV (46 cores) areas, where the sediment penetration is 11.46 m or less. Thirty-six regional cores (REG) were collected from outside BH and AAV areas in Middle Valley (Fig. 2).
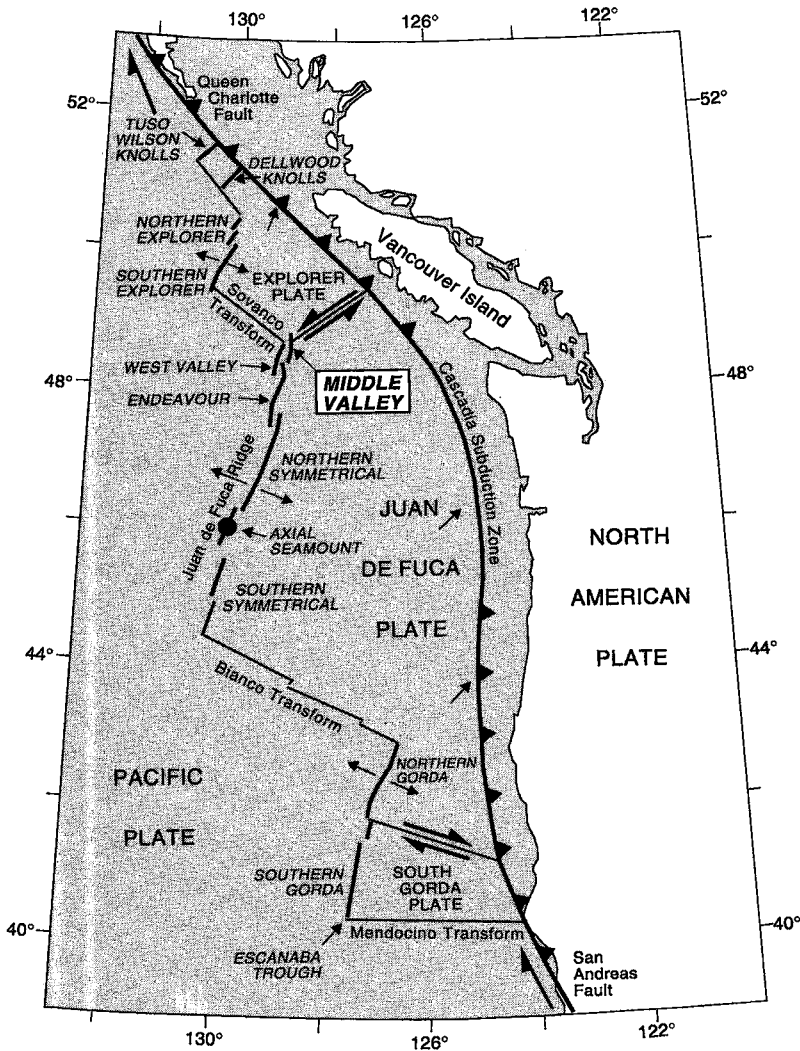

FIG. 1. Map of the Juan de Fuca Ridge system showing the main tectonic elements and the location of Middle Valley at the northern extremity of the Ridge.
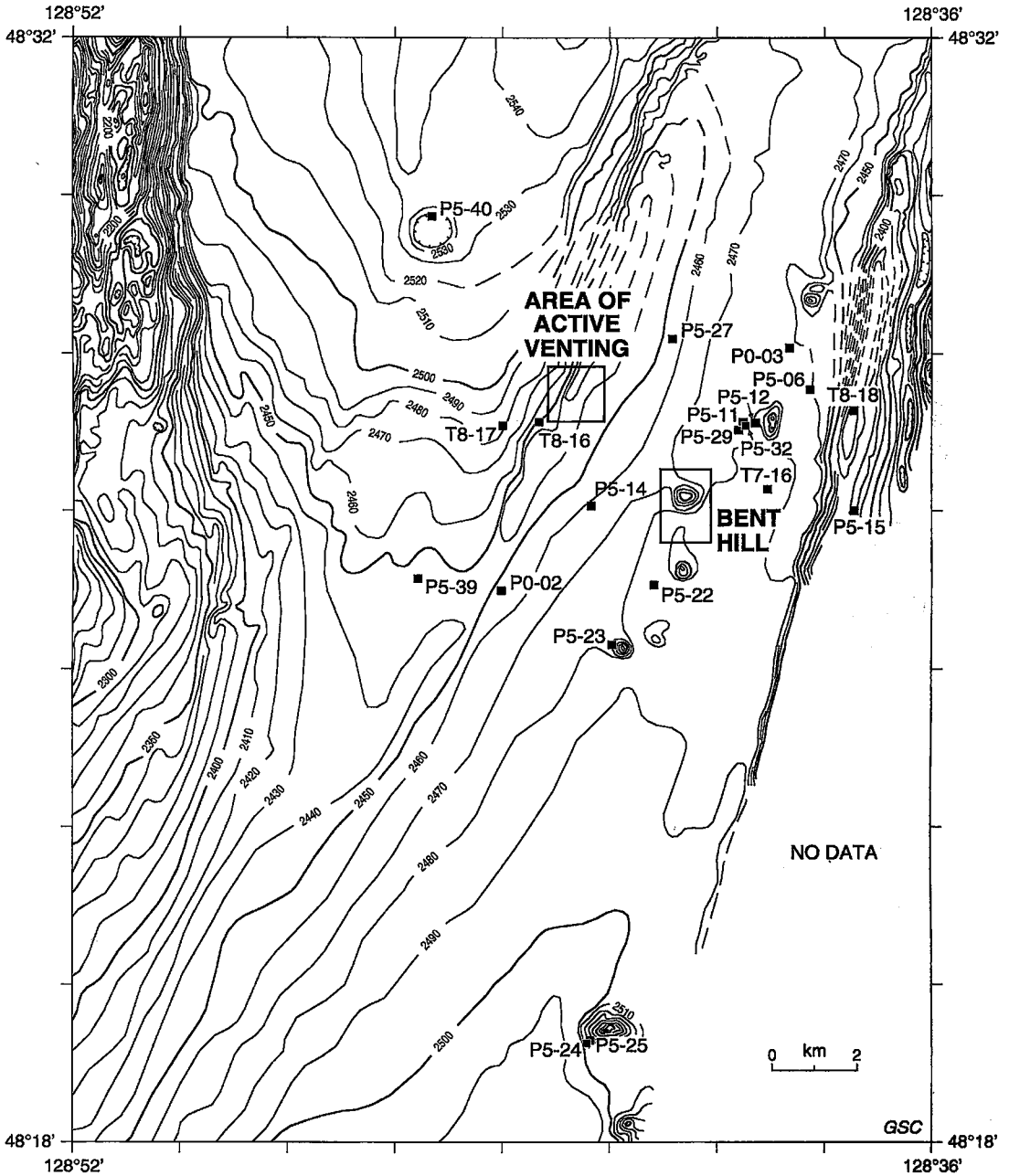
FIG. 2. Seabeam bathymetric map of Middle Valley (Davis & Sawyer 1987) showing the location of Regional cores, the Area of Active Venting (AAV) and the Bent Hill (BH) sulfide deposit. Because of the high number of cores collected at BH and AAV, they are plotted at an expanded scale in Figures 3 and 4, respectively.

SAMPLING AND ANALYTICAL METHODS

Sediment cores were collected with shipboard piston, gravity and boomerang corers, and by ALVIN push corers. The location of all cores, except those with the prefix PAR85, was determined by an Oceano transponder net that was positioned in absolute space by a Global Positioning System (GPS). Sample prefixes refer to the ship's name and the collection year (*i.e.*, PAR85: PARIZEAU, 1985; TUL87: TULLY, 1987, *etc.*). X-radiography was performed on all cores, and they were subsequently described in detail. Most cores were sampled continuously along their length for bulk chemical composition, and discontinuously for petrography, mineralogy and isotope chemistry. Core samples were vacuum-impregnated with epoxy and slabbed, and polished thin sections were prepared of oriented samples. Samples for clay mineralogy were first freeze-dried, and sand and silt fractions were then separated using a 63 μm sieve. To minimize the effects of salt on clay flocculation, the <63 μm fraction was washed four times to dissolve all the salt before separating the <2 μm clay fraction by settling through a column of de-ionized water. The clay fraction was analyzed by X-ray diffractometry on slides using methods described by Chamley (1971) and Holtzapffel (1985). X-ray diffractograms were obtained with a General Electric XRD-3 diffractometer using copper radiation at 45 kV and 16 mA, and a scan rate of 2° 2θ per minute for the 2θ range of 2.5 – 25°.

Cores analyzed for bulk chemical composition were sampled continuously at 10–20 cm intervals. Samples were oven dried at 110°C, pulverized and ground to <200 mesh, and analyzed at the Geological Survey of Canada after fusing 0.5 g of sample with lithium metaborate and dissolving the fused sample in 5% HNO_3. Samples of selected cores were weighed before and after drying to determine the water content and porosity. Analytical methods are: Induction Coupled Plasma – Emission Spectrometry: SiO_2, TiO_2, Al_2O_3, K_2O, Na_2O, CaO, MgO, P_2O_5, MnO, Fe_2O_3(total), Ba, Ag, Be, Co, Cr, Cu, La, Ni, Pb, Sr, V, Yb and Zn; Atomic Absorption Spectrometry: As, Sb, Se, Cd, Hg; anion chromatography (Dionex): Cl and F; combustion and wet-chemical methods: FeO, H_2O, CO_2 and S.

Samples selected for sulfur isotope analyses were dried in a nitrogen atmosphere, and sulfide and sulfate minerals were separated using a combination of physical and chemical methods [see Goodfellow & Blaise (1988) for methods of sulfur extraction]. Values of $\delta^{34}S$ (2σ = 0.2‰) were measured on a VG Micromass 602 mass spectrometer at the University of Ottawa. Results were standardized to the Canyon Diablo troilite using the McMaster reference standards of Rees (1978).

Carbonate concretions and cement were separated physically and purified chemically, and analyzed for $\delta^{13}C$ (2σ = 0.1‰) and $\delta^{18}O$ (2σ = 0.1‰) values at the University of Ottawa, and for $^{87}Sr/^{86}Sr$ at Geochron Laboratories, Cambridge, Massachusetts. Barite, talc and Mg-rich smectite-group minerals were separated by physical methods; $\delta^{18}O$ (2σ = 0.1‰) values for barite and silicate minerals, and δD values for silicate minerals, were determined at Geochron Laboratories.

REGIONAL AND LOCAL GEOLOGY

Stratigraphy and sedimentology

The sedimentary sequence penetrated by 12-m cores consists of Holocene and latest Pleistocene interbedded hemipelagic and turbiditic sediment (Goodfellow & Blaise 1988). Within this interval, six distinctive units, herein referred to as Units 1 to 6, have been recognized on the basis of color and sedimentary textures (Goodfellow & Franklin 1993). Unit 1 consists of water-saturated, oxidized, brownish grey hemipelagic sediment that occurs 0–12 cm below the seafloor. Unit 2 underlies Unit 1 and is a yellow olive-grey hemipelagic sediment that is commonly parallel-laminated. Unit 2 contains abundant foraminifers, diatoms, radiolarians and nannofossils. Turbiditic silt laminae and beds characterized by sharp bases and diffuse tops occur in Unit 2, but they are not common. Unit 3 is a tan olive-grey hemipelagic sediment that is typically bioturbated and commonly interbedded with turbiditic silt and fine-grained sand. The turbiditic beds are typically parallel-laminated and less commonly cross-laminated, with layers that display sharp and scoured bases.

Unit 4 is composed of light olive-grey hemipelagic sediment that is interbedded with olive-grey hemipelagic sediment and turbiditic silt and sand. Medium to dark grey turbiditic beds display sharp and commonly scoured bases, and fine upward into silty mud.

Unit 5 consists of dark grey hemipelagic sediment with horizontal zoophycos worm burrows. The upper contact with Unit 4 is typically sharp and represented in some cores by a disconformity. The lateral continuity of Unit 5, particularly in the AAV, makes it a useful time-stratigraphic "marker unit". Unit 5 is underlain by grey to olive grey hemipelagic sediment of Unit 6 that is interlaminated in places with turbiditic silt. The turbidites are medium to dark grey, display sharp bases and diffuse tops, fine upward, and are delicately laminated.

Microfossils are most common in the fine-grained olive grey muds and consist of foraminifers, nanofossils, diatoms and radiolarians. Planktonic foraminifers (*Globigerina buloides*) in carbonate-rich beds located at 75–77 cm depth in PAR 85–28 have been ^{14}C dated at 13,490 (± 210) aBP (Goodfellow & Blaise 1988). Planktonic foraminifera (*Globigerina buloides*) at
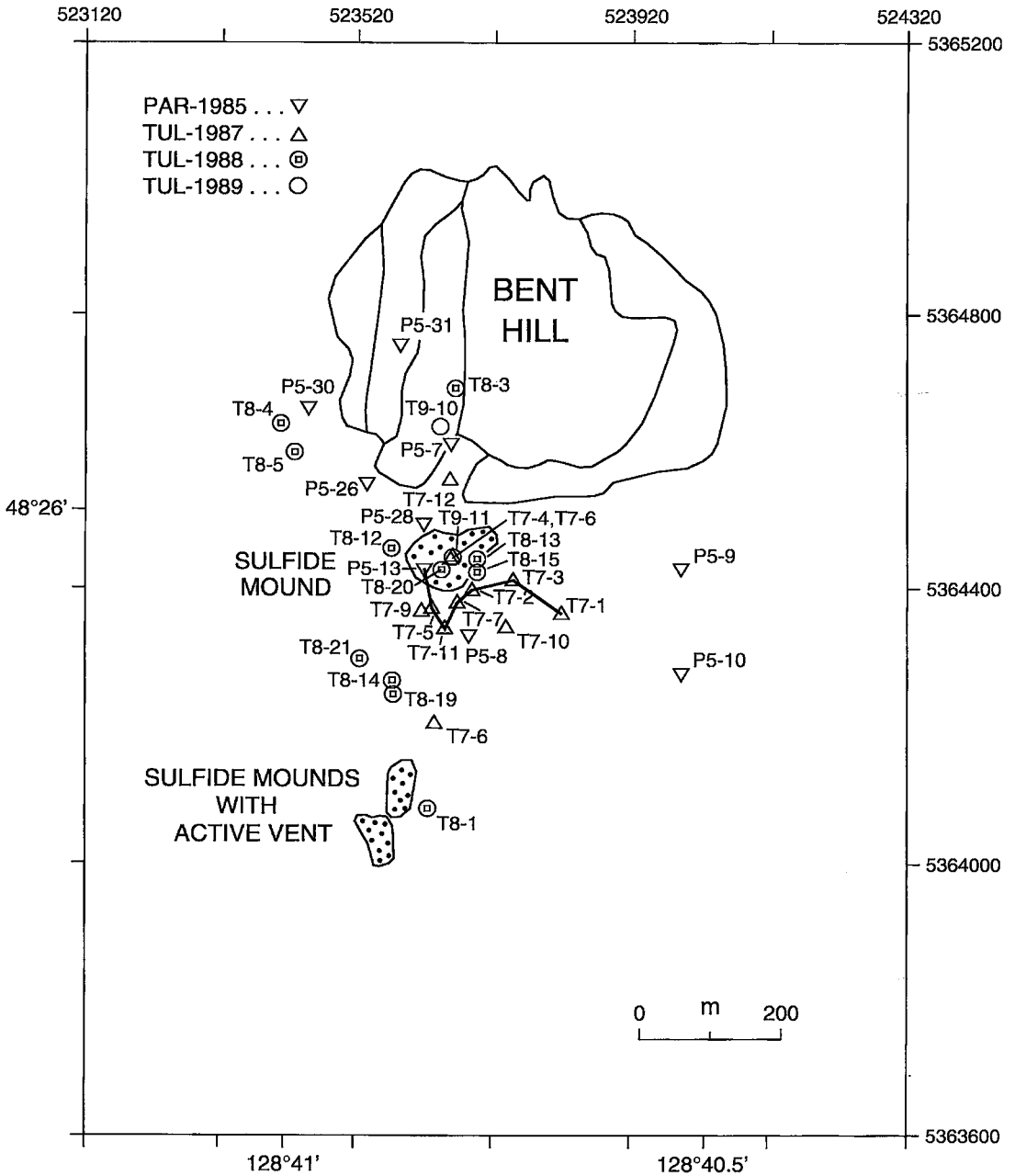
FIG. 3. Map showing Bent Hill, the sulfide mound near the southern flank, and the southern sulfide mounds with a hydrothermally active anhydrite–sulfide chimney. Cores collected between 1985 and 1988 at or near Bent Hill also are plotted. P5: PARIZEAU85; T7: TULLY87; T8: TULLY88.

64–66 cm, 78–79 cm, 160–162 cm and 847–848 cm in PAR 85–34 have been dated at 10,260($\pm$ 2,470), 12,090($\pm$ 170), 13,900($\pm$ 180) and 21,010($\pm$ 280) aBP (this report, Goodfellow & Blaise 1988). Average rates of sedimentation for the Holocene calculated using these dates are 5.5 – 5.8 cm ka^{-1} for core PAR 85–28 on top of BH, and 6.4–6.6 cm ka^{-1} for core PAR 85–34 in the AAV. The slower rate of sedimentation in core PAR85–28 indicates that BH was a positive bathymetric feature during most of the Holocene. Average rates of sedimentation for Holocene and Late Pleistocene sediment in core PAR85–34 are much higher (40 cm ka^{-1}) because of the influx of turbidites in the Late Pleistocene.

BENT HILL

Geological setting

Bent Hill (BH) forms one of a chain of sediment mounds that are oriented approximately north–south and are parallel to extensional faults bounding the Middle Valley rift (Fig. 2). BH is a 60-m high by 400-m wide sediment structure (Fig. 3) that is abruptly truncated to the west by north–south faults, producing fault steps and scarps (Goodfellow & Franklin 1993). Near the southern margin of BH is a 35-m high by 100-m wide sulfide mound that consists of sulfide rubble near the summit and interbedded hemipelagic
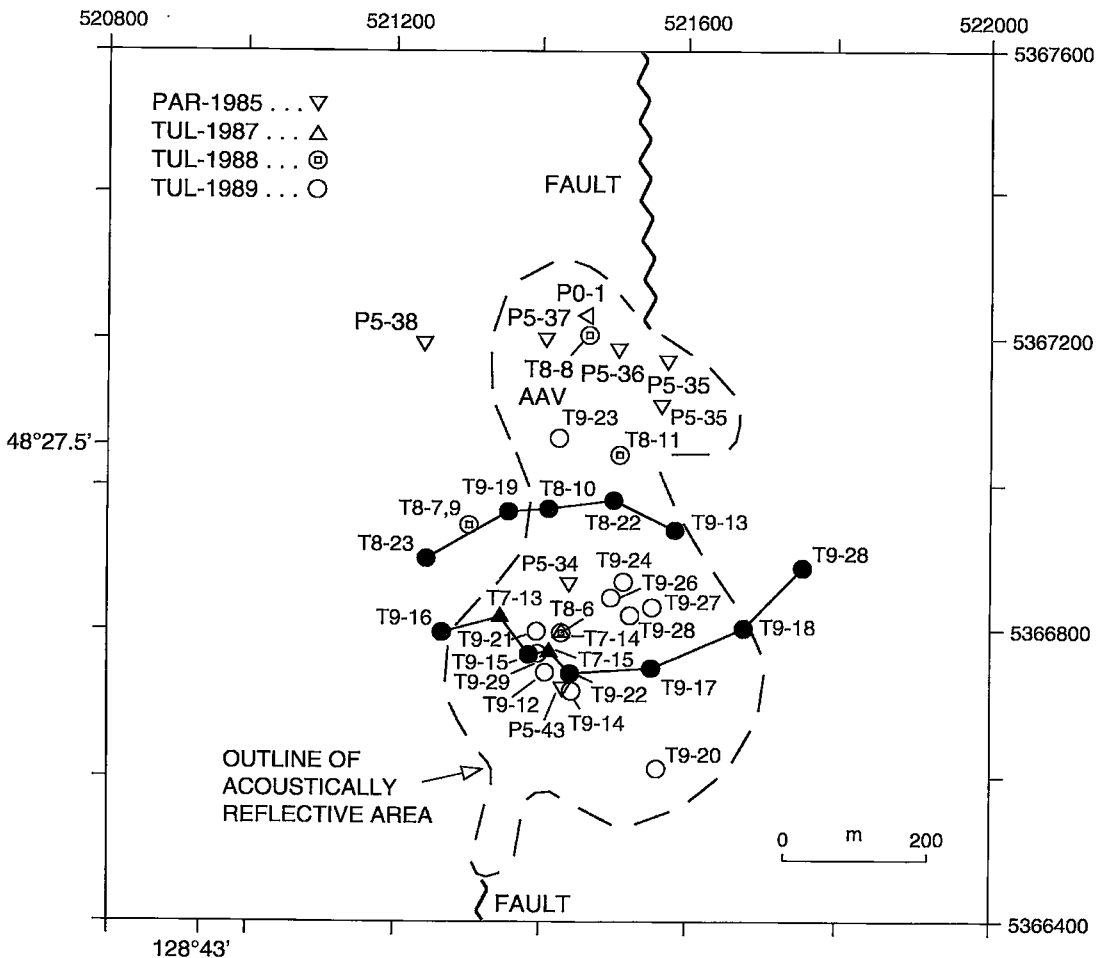

FIG. 4. Map of the Area of Active Venting (AAV) showing the outline of the acoustically reflective area, positions of shallow cores, and the location of two cross-sections presented in Figures 6 and 7. P5: PARIZEAU85; T7: TULLY87; T8: TULLY88.

and clastic sulfide sediment on the flanks. About 330 m south of BH are two smaller 20-m high sulfide mounds with an anhydrite chimney near the summit of northernmost one that is actively venting fluids at 265°C (Franklin *et al.* 1992).

Stratigraphy and sedimentology

Cores collected from 1985 to 1989 are located on a map of the BH area showing the limits of sediment and sulfide mounds (Fig. 3). Most of the cores are clustered along the western and southern flanks of BH, at the summit and margins of the sulfide mound, and south of the sulfide mound. Core TUL88–01 is near the southern sulfide mound on which an actively venting anhydrite–sulfide chimney was observed and sampled in 1990 by the ALVIN submersible.

AREA OF ACTIVE VENTING (AAV)

Geological setting

The AAV is a 800 m by 400 m vent field (Fig. 4) situated 2.4 km west-northwest of BH, on the downthrown side and immediately east of an extensional fault that is parallel to the rifted margins of Middle Valley. This vent field hosts at least 15 vent sites that are actively discharging hydrothermal fluids from anhydrite chimneys situated on sediment mounds (Turner *et al.* 1991, Franklin *et al.* 1992, Lydon *et al.* 1992). High-resolution SeaMARC 1A images (Goodfellow & Franklin 1993) show that the AAV occurs near a right-lateral offset of a rift-parallel extensional fault that penetrates the seafloor. The actual vent-sites and associated hydrothermal mounds are oriented northwest along what may be a conjugate set of orthogonal extensional faults.

The AAV corresponds to a bathymetric low and an area of high acoustic reflectivity outlined by a SeaMARC 1A side-scan sonar survey of the area (Goodfellow & Franklin 1993). The source of high reflectivity is a roughness caused by the formation of mounds, the sedimentation of hydrothermal sulfide, sulfate and silicates near vents, and the alteration of the uppermost sediment by hydrothermal fluids. The correspondence between high heat-flow (Davis & Villinger 1992), hydrothermal alteration, hydrothermal pore-fluids (Lydon *et al.* 1991) and high acoustic reflectivity suggests that this feature was formed by the advection of hydrothermal fluids through the sedimentary sequence.

TABLE 1. MINERALOGY OF UNALTERED BULK SEDIMENT FROM CORE TUL89D–28, AS DETERMINED BY X–RAY–DIFFRACTION ANALYSIS

Section	Sample	Depth (cm)	Mineral Assemblage
01	02X	26.0	QTZ, Pl, Chl, mica
01	03X	74.0	QTZ, Pl, Cal, Chl, mica
02	04X	49.0	QTZ, Pl, Cal, Chl, mica
02	05X	84.0	QTZ, Pl, Cal, Chl, mica
02	06X	124.0	QTZ, Pl, Cal, Chl, mica, amphibole
03	07X	20.5	QTZ, Pl, Cal, Chl, mica
03	08X	88.0	QTZ, Pl, Cal, Chl, mica
03	09X	104.0	QTZ, Pl, Cal, Chl, mica
04	10X	31.0	QTZ, Pl, Cal, Chl, amphibole
04	11X	111.0	QTZ, Pl, Cal, Chl

Capitalized mineral name represents a major phase. Uncapitalized mineral name represents a minor or trace phase.

Stratigraphy and sedimentology

Cores from the AAV (Fig. 4) are stratigraphically similar to regional cores, but individual units have been variably altered by hydrothermal fluids. Despite the overprinting effects of hydrothermal alteration, the original depositional units summarized in Goodfellow & Franklin (1993) can be identified except in a few cores near the locus of discharge of hydrothermal fluid, where the subtle differences in color of individual units have been destroyed by hydrothermal alteration.

Stratigraphic units through the AAV are laterally continuous but variable in thickness. The thicknesses of units 2, 3 and 4 generally increase from the periphery to the center of the vent field (Goodfellow & Franklin 1993). This increase indicates that the AAV has subsided after deposition of the worm-burrowed "Marker Unit" (Unit 5), a distinctive medium grey hemipelagic mud that is typically less than 10 cm thick and is composed of up to six horizontal to subhorizontal zoophycos worm burrows.

MINERALOGY

Unaltered hemipelagic and turbiditic sediment

Bulk turbiditic sediment analyzed by X-ray diffrac-

TABLE 2. XRD MINERALOGY OF <2 μm CLAY FRACTION,
UNALTERED HEMIPELAGIC SEDIMENT

TUL89D Core and Section		Depth (cm)	Description	Mineralogy
16	2	62-67	Olive grey mud interbedded with tan grey mud	ILL, CHL, qtz, ab
	2	113-118	Light to medium olive grey, weakly indurated mud	ILL, CHL, qtz, ab, amphibole
	3	70-75	Dark grey mud with sub-horizontal worm burrows	ILL, CHL, qtz, ab, amphibole
	3	114-119	Light olive grey and tan grey hemipelagic mud	ILL, CHL, qtz, ab, amphibole
18	5	115-120	Brilliant greenish-grey, moderately indurated mud	ILL, CHL, qtz, ab, amphibole
	5	30-35	Light greenish-grey, weakly indurated mud	ILL, CHL, qtz, ab, amphibole
	4	60-65	Tan grey, weakly indurated hemipelagic mud	ILL, CHL, qtz, ab, amphibole
	1	34-40	Medium olive grey, weakly indurated, clumpy mud	ILL, CHL, qtz, ab, amphibole
28	4	55-60	Med.-light olive greenish-grey mud, weakly indurated, whitish gypsum/anhydrite	CHL, ILL, ab, qtz, amphibole
	4	111-116	Light olive grey, moderately indurated mud with coarser grained authigenic minerals, violent reaction with NaOAc	CHL, ILL, ab, qtz, amphibole
	3	80-85	Medium greenish-grey mud immediately above dark grey mud unit with subhorizontal worm burrows	CHL, ILL, ab, qtz, amphibole
	2	17-23	Light olive grey mud interbedded with medium greenish-grey mud	CHL, ILL, ab, qtz, amphibole

tion (XRD) contains, in order of decreasing abundance, quartz, plagioclase, muscovite, chlorite, amphibole and minor biogenic calcite (Table 1). In addition, turbiditic sand and silt contain variable but generally minor amounts of magnetite, zircon, titanite and apatite. The quartz in samples examined by scanning electron microscopy (SEM) occurs as equant, abraded grains, whereas feldspar grains are equant to elongate. Detrital feldspars consists mostly of calcic plagioclase (up to An$_{70}$), K-feldspar and minor albite. Chlorite and muscovite, the most common phyllosilicates, occur as irregular grains or as clusters of ragged flakes indicating a detrital origin. Detrital chlorite analyzed by SEM–EDX (energy-dispersion spectrometry) has a Fe/Mg weight ratio greater than one.

Hemipelagic silt-clay consists of foraminifers, diatoms, radiolarians, nannofossils, detrital quartz, plagioclase, muscovite, chlorite and amphibole, and authigenic clay (Table 1; Goodfellow & Blaise 1988). The <2 μm fraction contains, in order of decreasing abundance, chlorite, an illite-group mineral, quartz, feldspar and amphibole (Table 2). No smectite was detected in cores remote from active vents in the AAV (cores TUL89D–18 and –28, Fig. 4).

Holocene sediments are relatively enriched in secondary clay (smectite-group minerals and irregular mixed-layer) compared to Late Pleistocene sediments, which contain a higher proportion of primary (chlorite and illite) clay minerals (Goodfellow & Blaise 1988). Patches and disseminations of black diagenetic Fe monosulfide occur throughout hemipelagic sediment and are most abundant in intervals rich in biogenic components.

Hydrothermally altered sediment

Representative samples of hydrothermally altered hemipelagic sediment were collected from cores TUL89D–22 and TUL89D–17 in the AAV to determine the mineralogy of the clay-size fraction near active vents (Fig. 4). Table 3 presents the predominant mineralogy of the clay-size fraction of sediment samples, as determined by X-ray diffractometry. The spatial distribution of Mg-rich smectite-group minerals (mostly saponite) in the clay fraction corresponds approximately to the alteration zone shown in Figure 5.

The subsurface geology and extent of hydrothermal alteration of the AAV are illustrated on two west–east cross-sections of the AAV (Figs. 6, 7). The southern cross-section (Fig. 6) spans at least two major vent-fields and associated zones of hydrothermal alteration. Hydrothermally altered sediments are more restricted on the northern cross-section (Fig. 7) because it intersects one vent-field. The stratigraphy on each cross-section is similar and consists of laterally continuous units that generally thicken above the "marker unit" toward the center of hydrothermal fluid dis-

TABLE 3. XRD MINERALOGY OF <2 μm CLAY FRACTION, HYDROTHERMALLY ALTERED HEMIPELAGIC SEDIMENT

TUL89D Core and Section		Depth (cm)	Description	Mineralogy
17	2	55-57	Light grey, moderately indurated hemipelagic mud	SMECTITE (saponite), Chl, Ill, trace qtz and feldspar
	3	12-15	Medium-grey, moderately altered mud	SMECTITE (saponite), Chl, Ill, trace qtz and feldspar
	3	47-49	Light to medium grey, moderately altered mud	SMECTITE (saponite), Chl, Ill, trace qtz and feldspar
	3	100-103	Medium-grey, moderately altered mud, slightly green	SMECTITE (saponite), Chl, Ill, trace qtz and feldspar
22	3	151-153	Medium olive grey, moderately indurated mud	SMECTITE GROUP, ILL, CHL, qtz, ab
	4	72-76	Light olive grey, highly indurated, altered mud	SMECTITE GROUP, ILL, CHL, qtz, ab, Cal
	4	118-123	Very dark grey, highly indurated, altered mud	SMECTITE GROUP, ILL, CHL, qtz, ab
	4	132-136	Yellowish-brown, highly indurated, altered mud	SMECTITE GROUP, ILL, CHL, qtz, ab
24	2	75-80	Medium olive grey, weakly indurated mud	SMECTITE GROUP, ILL, CHL, qtz, ab, amphibole
	2	133-138	Tan grey, weakly indurated mud	SMECTITE GROUP, ILL, CHL, qtz, ab, amphibole
	4	41-46	Light grey to olive grey, weakly indurated mud	SMECTITE GROUP, ILL, CHL, qtz, ab
	4	122-127	Medium olive grey to grey, mottled hemipelagic mud	SMECTITE GROUP, ILL, CHL, qtz, ab

charge. Unaltered olive grey hemipelagic sediments take on a blue-green hue (Zone II) and become pale grey (Zone I) and increasingly indurated, veined and laden with pyrite toward vent sites.

The blue-green alteration in both cross-sections is not pervasive but is commonly restricted to particular stratigraphic units owing to the low cross-strata permeability. Carbonate concretions occur in Zones I and II, but are most common near the boundary separating the two alteration zones. In the southern cross-section (Fig. 6), one core (TUL87B–15) has penetrated 80 cm
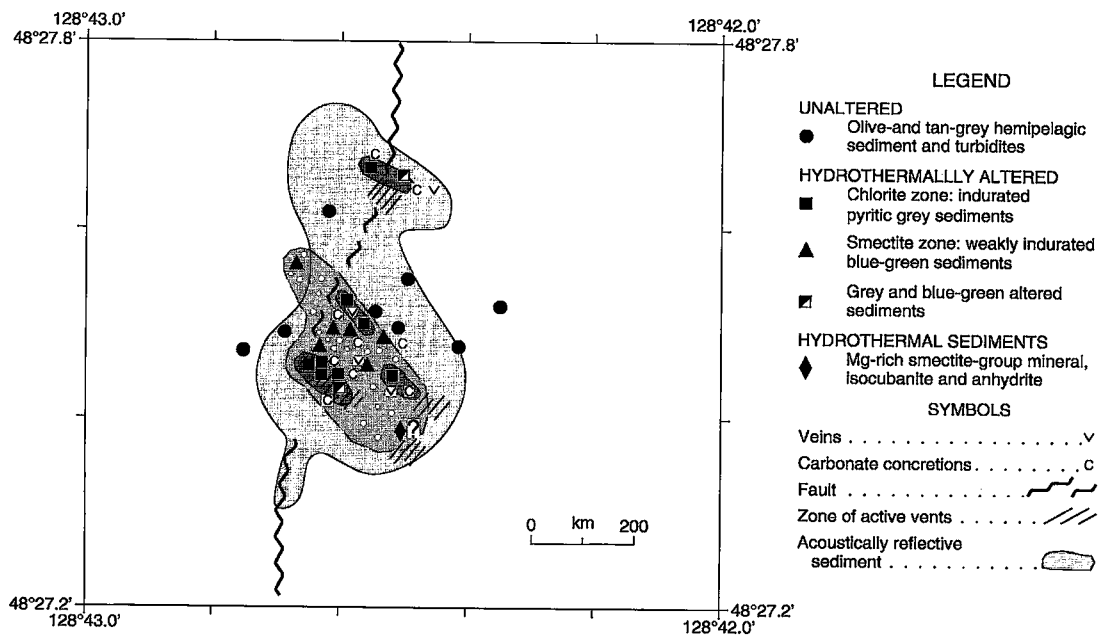
FIG. 5. Surface map of the Area of Active Venting (AAV) showing the distribution of active vents and associated hydrothermal mounds, zones of hydrothermal alteration, and acoustically reflective sediment.

of hydrothermal sediment that overlies olive grey hemipelagic sediment (Unit 2).

The Mg-rich smectite-group minerals in hydrothermally altered sediments occur in different forms: 1) as felted masses that line fractures cross-cutting altered hemipelagic sediment (Figs. 8a, b); 2) infilling and replacing foraminifers (Figs. 8c, d); and 3) replacing hemipelagic sediment (Fig. 8b). In the latter case, it commonly displays snow-flake and dendritic growth textures, and infills and partly replaces the matrix and overgrows coarser detrital grains. Figure 9 consists of SEM secondary electron images of hydrothermally altered sediment from core PAR85–34 that show the various forms of Mg-rich silicates. The Mg-rich smectite-group minerals display fibrous (Figs. 9a, c), felted (Figs. 9b, g, h), and felted botryoidal (Figs. 9d, e, f) textures. The morphology of these minerals supports an authigenic, hydrothermal origin. SEM emission spectra show that authigenic smectite-group minerals have high contents of Mg relative to Fe. Illite, albite and quartz also occur in altered sediment, but their common occurrence in unaltered hemipelagic sediment and the ragged morphology of chlorite and illite crystals favor a detrital origin.

Authigenic barite commonly occurs in hydrothermally altered sediment from the AAV, either in the form of rosettes of euhedral barite (Fig. 10a) or as discrete tabular crystals that enclose detrital grains

(Figs. 10b, c, d). Barite also occurs as radiating crystals associated with a network of amorphous silica (Fig. 10e). In one sample, barite crystals have nucleated on the surface of a foraminifer (Fig. 10f).

Hydrothermally altered sediment in the AAV also contains abundant gypsum that has infilled open spaces and replaced detrital grains. This gypsum forms pseudomorphs after primary anhydrite. The gypsum occurs in several forms: 1) splays (Fig. 11a), 2) a random network of needles (Fig. 11b), 3) isolated euhedral crystals (Fig. 11c) surrounded by detrital grains and within foraminifers (Fig. 11d), and 4) needles surrounded by euhedral pyrite (Fig. 11e). In Zone I, pyrite typically forms disseminated silvery bronze cubes that impart a speckled appearance to the pale grey altered hemipelagic sediment. Euhedral pyrite replaces diagenetic framboidal pyrite (Fig. 11f) in some samples, and it infills pore space and partly replaces detrital grains in turbiditic silt and sand.

Carbonate occurs in several forms in the altered sediment associated with the AAV: 1) concretions, 2) veins, 3) cement in worm burrows and detrital sediments, and 4) infillings and overgrowths on foraminifers. Carbonate concretions range in size from 1 cm to about 8 cm and are predominantly spheroidal or ovoid (Fig. 12a), although they commonly display irregular shapes, particularly where the carbonate infills and replaces branching worm burrows. The con-
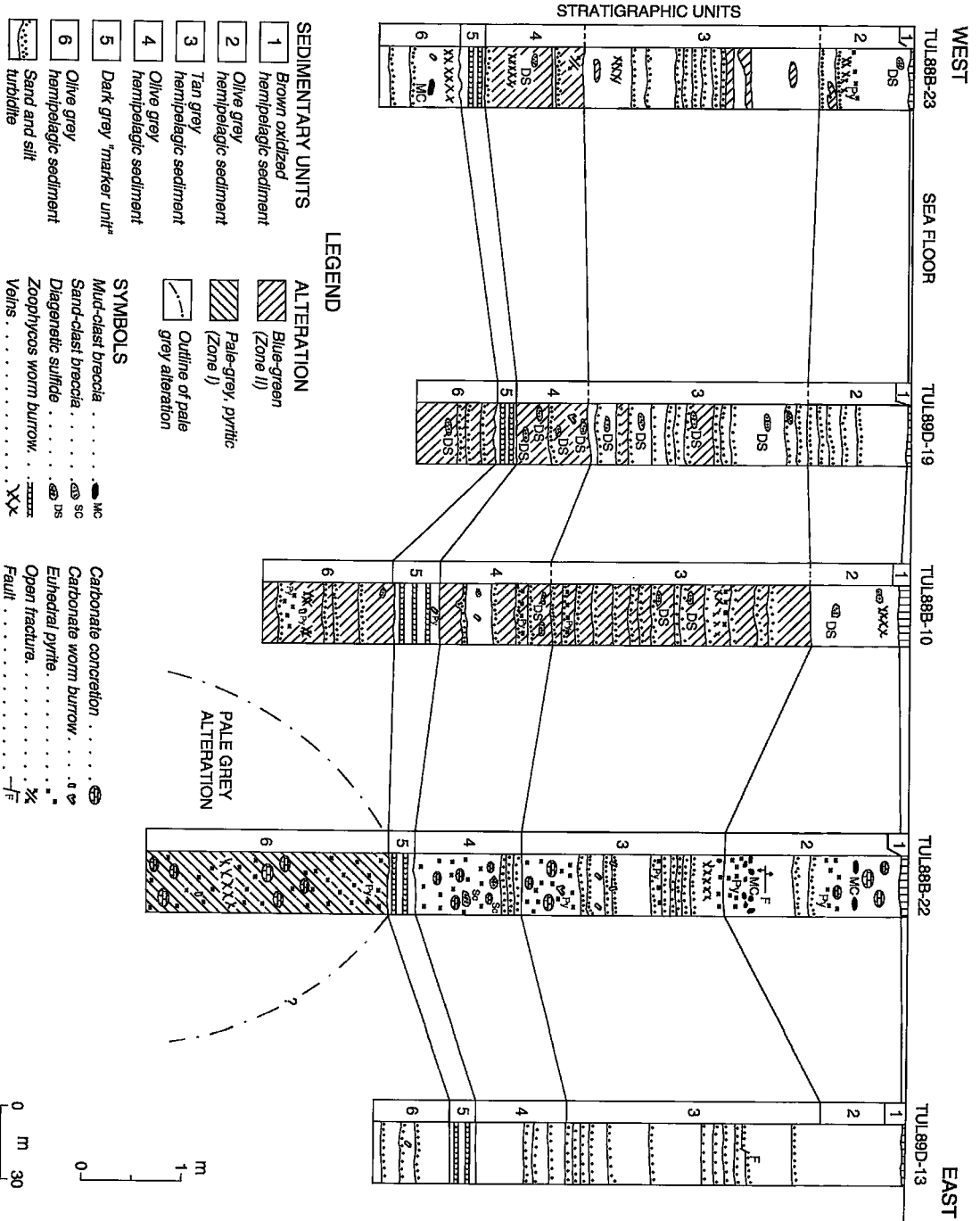
FIG. 6. East–west cross-section of the southern AAV illustrating the local stratigraphy, the distribution of hydrothermal Zones I and II, and hydrothermal structures and textures. Refer to Figure 4 for the location of cross-section.
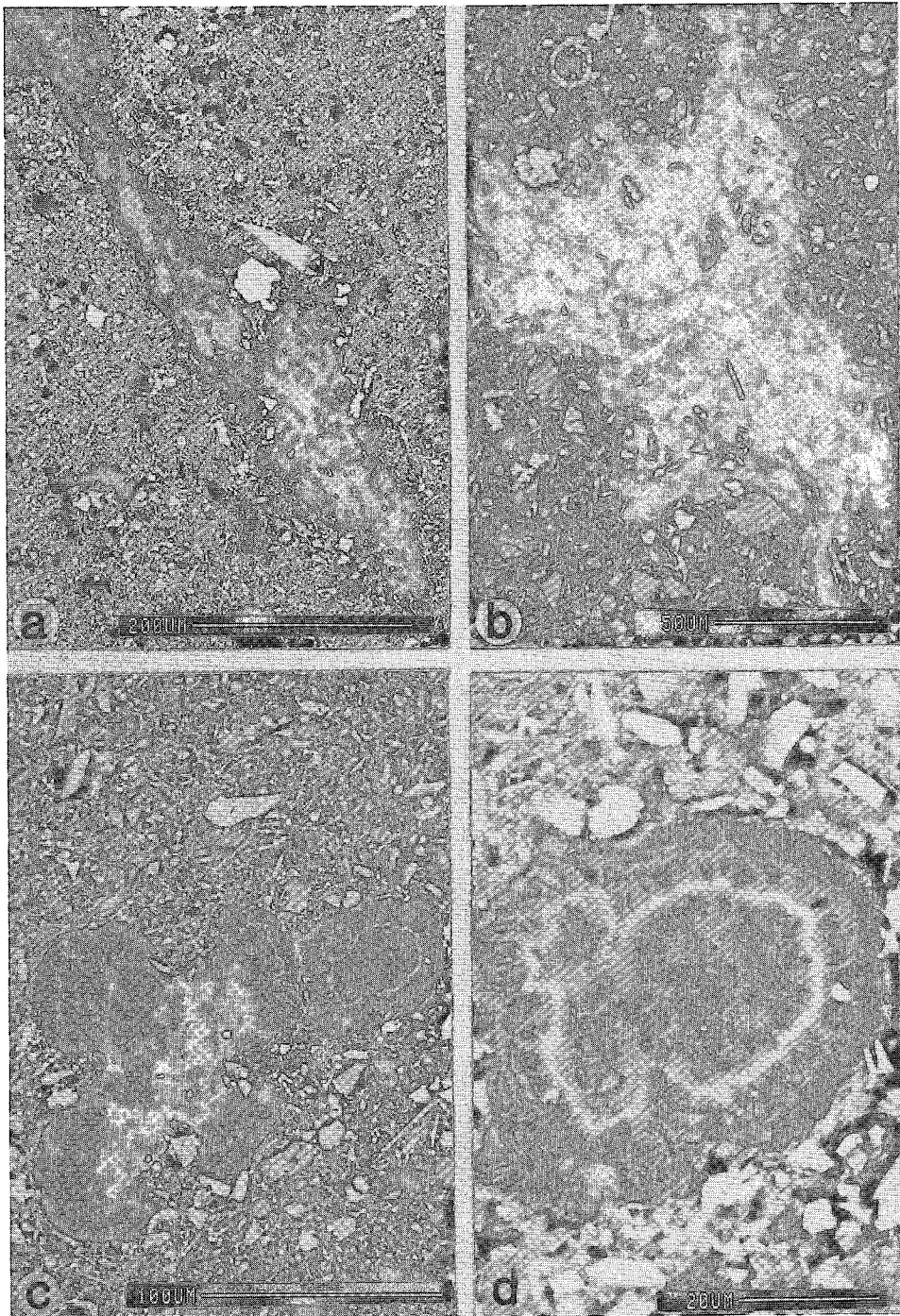
FIG. 7. East–west cross-section of the northern AAV illustrating the local stratigraphy, the distribution of hydrothermal Zones I and II, and hydrothermal structures and textures. Refer to Figure 4 for the location of cross-section.

FIG. 8. SEM secondary images of hydrothermally altered sediment, Middle Valley. (a) Fracture (black) rimmed by fibrous Mg-rich smectite-group mineral cutting hydrothermally altered sediment, TUL87B–15. (b) Blow-up of (a) showing felted masses of hydrothermal smectite replacing hemipelagic sediment. (c) Pseudomorphic concentric bands of fibrous Mg-rich smectite-group mineral infilling and replacing foraminifera in hydrothermally altered hemipelagic sediment, TUL87B–15. The smectite in each band displays a radial habit. (d) Blow-up of (c) showing the radial habit of Mg-rich smectite-group mineral within concentric bands.
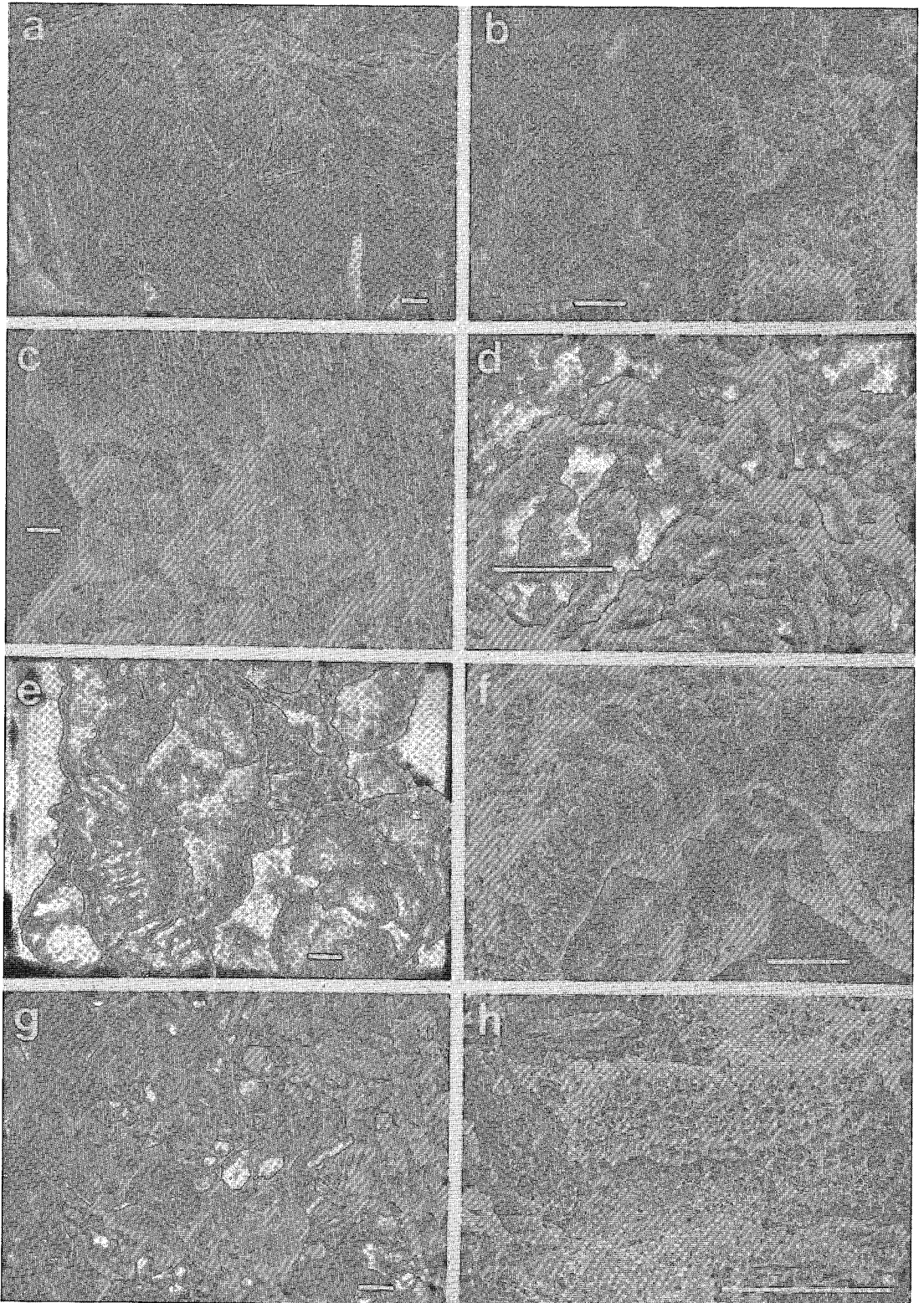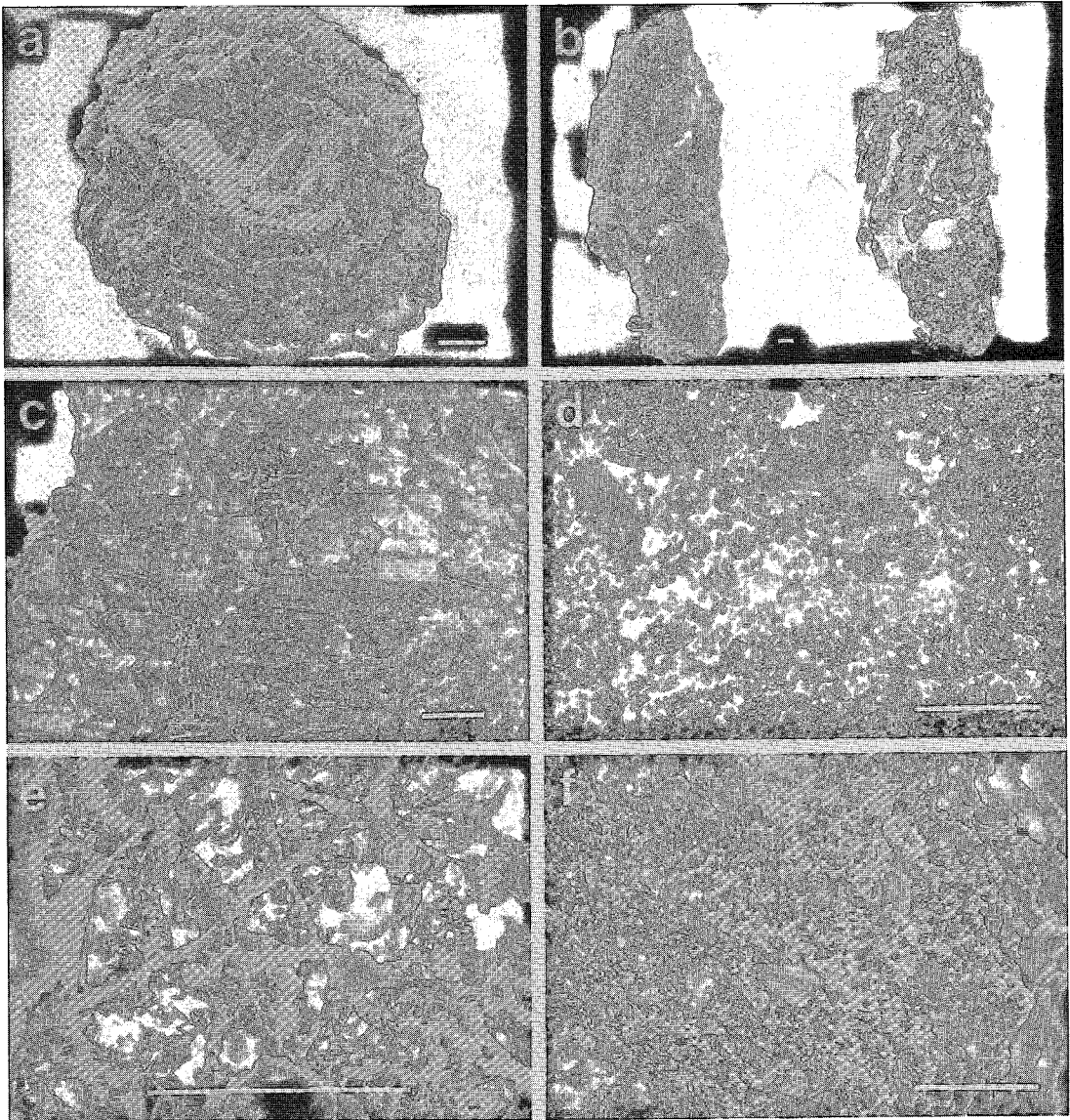
FIG. 10. SEM secondary image of hydrothermal barite and amorphous silica, core PAR85–34, Area of Active Venting. Scale bar: 50 µm. (a) Rosette of euhedral barite crystals in altered hemipelagic sediment, 670–672 cm. (b) Tabular barite enclosing detrital grains, 920–922 cm. (c) Euhedral barite growing in hemipelagic sediment, 570–572 cm. (d) Barite crystals growing in hemipelagic sediment with framboidal pyrite, 900–902 cm. (e) Radiating barite crystals and interconnected strands of amorphous silica in hemipelagic sediment, 110–112 cm. (f) Barite crystals on a foraminifer.

FIG. 9. SEM secondary images of hydrothermal Mg-rich silicates, core PAR85–34, 10–12 cm, Area of Active Venting. Scale bar: 20 µm. (a) Fibrous network of hydrothermal smectite growing in hemipelagic sediment. (b) Open felted masses of smectite-group mineral. (c) Fibrous network of smectite-group mineral. (d) Felted botryoidal smectite. (e) Side view of (d). (f) Open interlocking felted network of smectite-group mineral with grains of detrital sediment. (g) Felted mass of smectite-group mineral.
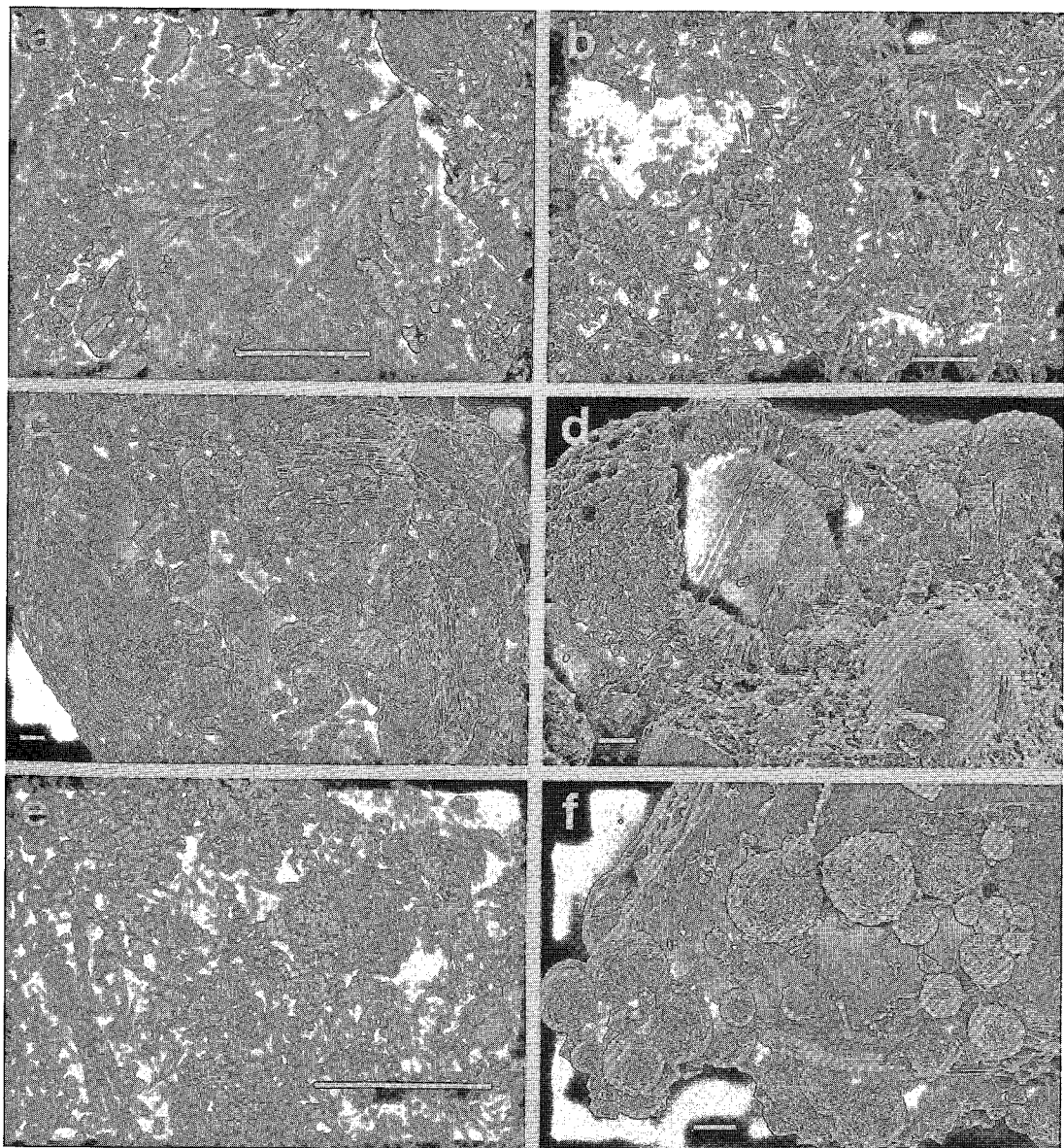
FIG. 11. SEM secondary images of hydrothermal gypsum and pyrite in hydrothermally altered sediment, core PAR85–34. Scale bar: 20 μm. (a) Splays of authigenic gypsum in hemipelagic sediment, 900–902 cm. (b) Random network of gypsum needles surrounded by detrital grains, 900–902 cm. (c) Euhedral crystal of gypsum infilling and encompassing detrital grains, 922–926 cm. (d) Euhedral crystal of gypsum in altered foraminifer, 920–922 cm. Foraminifer has been recrystallized and is now composed of radiating crystals of calcite. (e) Gypsum needles surrounded by framboids of pyrite cubes, 580–582 cm. (f) Framboids of pyrite growing on euhedral gypsum, 920–922 cm.

FIG. 12. Photograph and SEM secondary electron images of carbonate concretions, PAR85–34. Scale bar: 20 μm. (a) Photograph of a carbonate concretion with detrital grains on surface, 110–112 cm. (b) SEM secondary electron image of vein of euhedral calcite cutting carbonate concretion, 63–64 cm. (c) SEM secondary electron image of vein of euhedral barite cutting carbonate concretion, 63–64 cm. (d) SEM secondary electron image of euhedral barite on the surface of carbonate concretion, 110–112 cm.
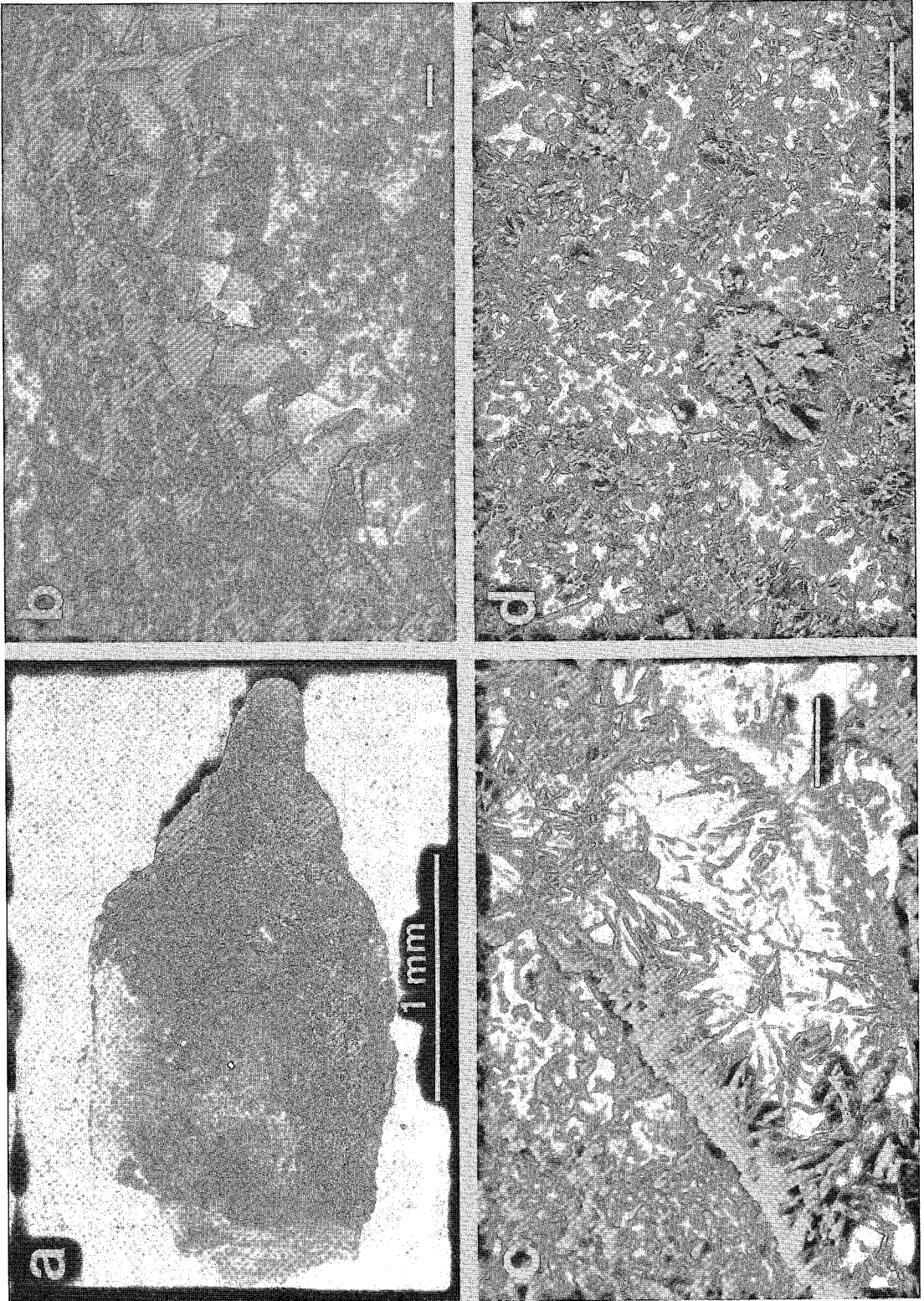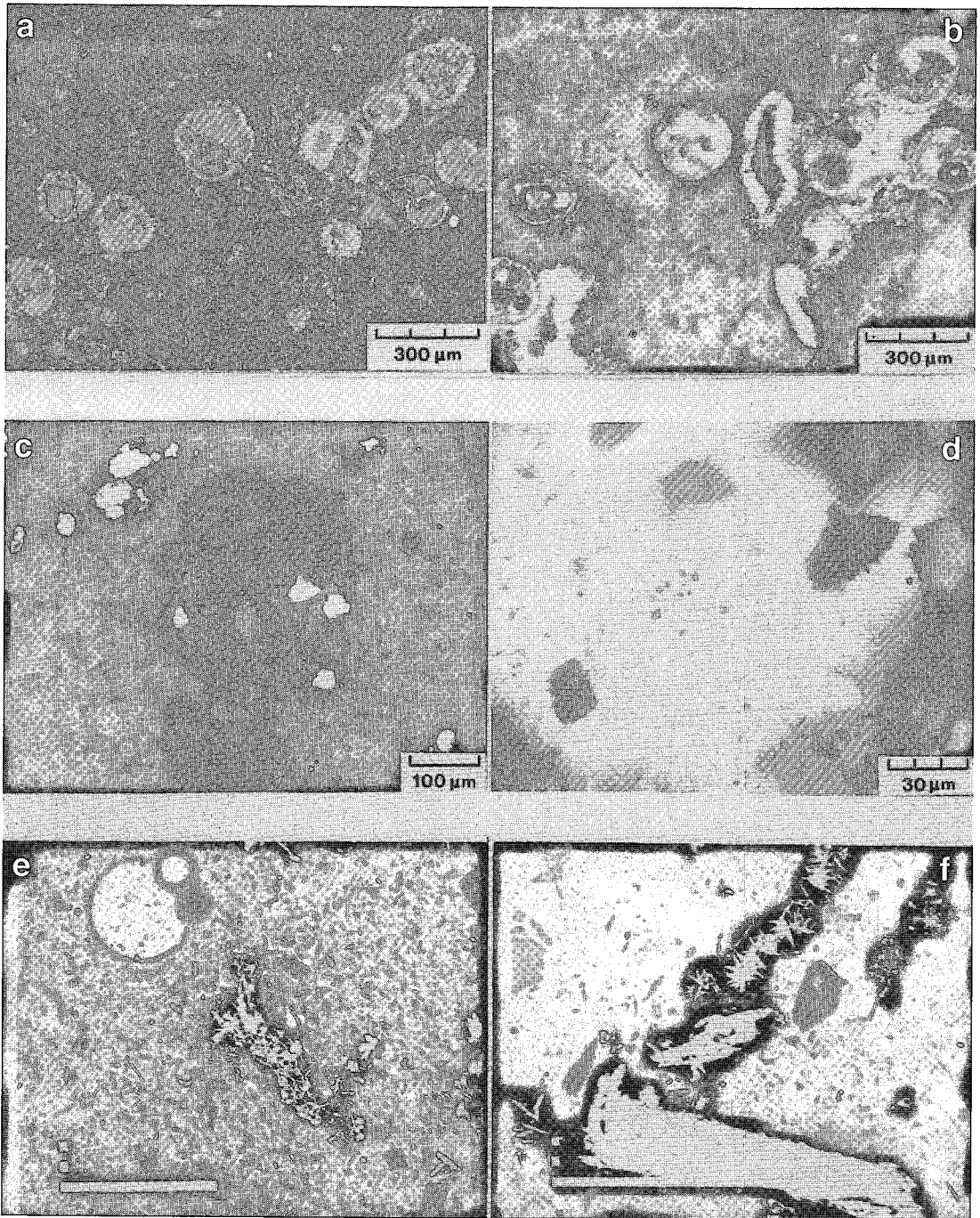
FIG. 13. Photomicrographs of foraminifers in various stages of hydrothermal alteration. (a, b) Recrystallized and overgrown foraminifera, sample TUL87B–15–03, 88–92 cm. (c) Authigenic pyrite accompanying recrystallized calcite, TUL87B–15–07–04, 82–86 cm. (d) Authigenic pyrite that penetrates foraminifer test structure, TUL87B–07–14, 82–86 cm. (e,f) Authigenic tabular pyrrhotite grains variably replaced by pyrite, sample TUL87B–07–04, 82–86 cm.

tact between concretions and the surrounding sediment is typically sharp and irregular. Some concretions are concentrically zoned, with an outer rim of fine-grained crystalline pyrite. Carbonate concretions contain smectite-group minerals and disseminated pyrite, which is finely intergrown with carbonate. Some carbonate concretions are cut by veins of coarse-grained euhedral calcite (Fig. 12b) and barite (Fig. 12c). Authigenic euhedral barite also forms on some carbonate concretions (Fig. 12d).

Foraminifers show progressive changes in texture, mineralogy and preservation from unaltered hemipelagic sediment to the core of Zone I. In Holocene hemipelagic sediment remote from hydrothermal centers, foraminifer structures and mineralogy are well preserved and are not altered by diagenetic or hydrothermal processes. Toward vent sites in the AAV, foraminifers show a progression from recrystallization to infilling, radial overgrowth and replacement by hydrothermal carbonate (Figs. 13a, b), euhedral pyrite (Fig. 13c) and other hydrothermal minerals such as barite. Pyrite penetrates into foraminifer tests in some samples (Fig. 13d) and replaces pyrrhotite plates in hemipelagic sediment (Figs. 13e, f). Recrystallization, infilling and overgrowth of foraminifers are most common near the transition between Zones I and II, where carbonate concretions and carbonate-cemented worm burrows are most abundant. Toward the core of Zone I, foraminifers become increasingly more corroded and are ultimately destoyed, presumably owing to dissolution by hydrothermal fluids.

GEOCHEMISTRY

Unaltered hemipelagic and turbiditic sediment

Bulk compositions were determined for regional cores PAR85–09, PAR85–14, PAR85–19, PAR85–24 and PAR90–02. Summary statistics for the compositions of 84 samples of regional cores are presented in Table 4. Mean and median values are presented because the frequency distribution is skewed for some elements owing to anomalously high contents of transition metals in the oxidized surface-layer. The Na_2O content includes Na in NaCl that precipitated from pore water during the desiccation of the samples. The samples were not washed prior to drying because of possible dissolution of metastable iron monosulfides and anhydrite, and the difficulty of recovering fine (<0.1 μm) clays during the filtration of suspended sediment.

Three broad groups of elements have been defined for unaltered hemipelagic and turbiditic sediments using R-mode factor analyses. Group 1 consists of the oxides and elements SiO_2, Al_2O_3, TiO_2, MgO, P_2O_5, K_2O, Sr, Rb, Cr, Nb, La, Y, Yb, and Zr that occur in detrital minerals quartz, plagioclase, chlorite, apatite,

TABLE 4. CHEMICAL COMPOSITION OF UNALTERED HEMIPELAGIC AND TURBIDITIC SEDIMENT REMOTE FROM HYDROTHERMAL VENTS, MIDDLE VALLEY

Element	Mean	Median	C.V.
SiO_2	45.8	52.8	0.05
TiO_2	0.79	0.78	0.11
Al_2O_3	15.0	15.3	0.05
FeO	3.36	3.35	0.26
Fe_2O_3	3.39	3.39	0.28
MnO	0.12	0.11	0.41
Na_2O	3.62	3.49	0.14
K_2O	2.50	2.49	0.11
CaO	4.80	4.74	0.30
MgO	3.30	3.31	0.08
P_2O_5	0.19	0.19	0.11
CO_2	2.01	1.85	0.49
C(org.)	0.63	0.51	0.52
H_2O	4.68	4.45	0.15
S	0.10	0.06	1.33
Ba	914	685	0.62
Sr	278	280	0.19
Rb	87	89	0.11
V	135	130	0.08
Zn	131	110	0.43
Cu	53	48	0.33
Pb	13	14	0.41
Ni	57	49	0.41
Co	23	22	0.14
Cd	<1.5	<1.5	-
Mo	1.1	1.0	0.31
As	7.6	5.3	1.74
Sb	1.4	1.0	0.66
Hg	130	95	0.83
Se	0.88	0.70	0.79
Cr	62	57	0.23
Nb	9.4	9.5	0.49
Y	22	21	0.12
Yb	2.1	2.0	0.14
Zr	144	140	0.19
B	68	66	0.12
Be	1.76	1.70	0.15

C.V.: coefficient of variation. Concentrations of all oxides, S and C(org.) are expressed in wt.%. Concentrations of all elements are expressed in ppm, except for Hg (ppb). Number of samples: 84.

magnetite, titanite and zircon. These elements display statistically significant covariations, with correlation coefficients between 0.5 and 0.75 at the 95% confidence level. Within the detrital fraction, SiO_2 is most abundant in turbiditic silt and sand, whereas Al_2O_3, TiO_2, K_2O and MgO are most abundant in hemipelagic silty clay that consists mostly of illite-group minerals, muscovite and chlorite. The bulk chemical composition of elements bound in detrital minerals is
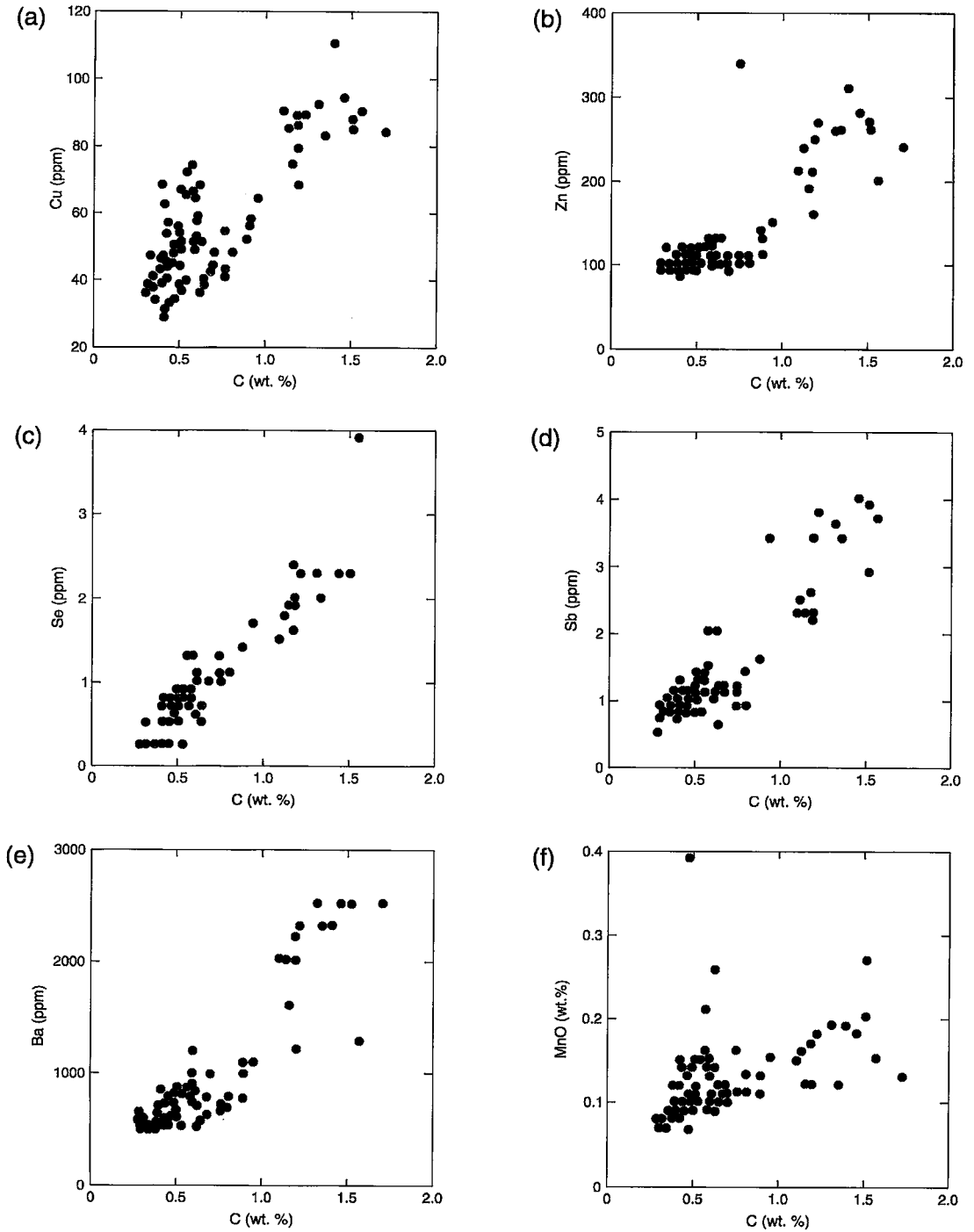
FIG. 14. Binary plots of a) Cu, b) Zn, c) Se, d) Sb, e) Ba and f) MnO with organic C in hemipelagic sediment remote from hydrothermal centers, Middle Valley.

dependent, therefore, on grain size and style of sedimentation.

Group 2 consists of CaO, CO_2, Sr and MnO, and is attributed to biogenic carbonates. Group-3 elements include most of the transition metals (*e.g.*, Zn, Cu, Ni, Co, V, Se, Sb, Mn and Fe) that are enriched in the brown, oxidized surface-layer (Unit 1). Other elements enriched in this surface layer are organic C, Ba and B. The transition metals form either Fe and Mn oxyhydroxides or are adsorbed to the surfaces of these minerals. The positive correlation of most transition metals with organic C (Fig. 14) most likely reflects the high content of organic matter in the oxidized surface-layer, and the coupled diagenetic reactions involving the bacterial oxidation of organic C and the reduction of Fe with depth. The inverse correlation of FeO with Fe_2O_3 (Fig. 15) attests to the reduction of ferric Fe during diagenesis. Elements sorbed onto oxyhydroxide surfaces and released to pore waters during the dissolution of Fe and Mn oxyhydroxides diffuse upward and are partly resorbed to oxidized surface sediments, or are precipitated with diagenetic sulfides. The highly positive correlation of Ba with organic C suggests that Ba was accumulated by biogenic processes. B was most likely enriched by sorption onto clay minerals (Spivack *et al.* 1987).

Hydrothermally altered sediment

Zone I is generally enriched in MgO, S, Ba, Zn, Cu, Pb, As, Sb, Se, Hg and Mo, and depleted in CaO, CO_2

TABLE 5. SUMMARY STATISTICS FOR HYDROTHERMALLY ALTERED SEDIMENTS, AAV, MIDDLE VALLEY

Element (wt. %)	Mean	Min.	Max.	C.V.	N	Mean (unalt.)
SiO_2	51.80	34.1	59.5	0.05	314	45.8
TiO_2	0.79	0.51	0.99	0.10	314	0.79
Al_2O_3	14.7	1.50	16.40	0.08	314	15.0
Fe(t)	4.93	3.50	9.16	0.09	314	5.26
FeO	3.05	n.d.	12.0	0.71	218	3.36
Fe_2O_3	1.73	n.d.	5.3	0.88	218	3.39
MnO	0.10	0.05	0.49	0.41	314	0.12
Na_2O	3.46	2.14	5.70	0.14	314	3.62
K_2O	2.52	1.09	3.63	0.16	314	2.50
MgO	3.81	0.56	11.9	0.39	314	3.30
CaO	4.79	0.67	22.4	0.46	314	4.80
P_2O_5	0.20	0.14	0.43	0.19	314	0.19
H_2O	2.54	n.d.	8.60	0.65	224	4.68
CO_2	2.30	0.00	16.60	0.72	312	2.01
C	0.48	0.10	2.00	0.68	312	0.63
S	1.27	0.26	6.52	0.78	314	0.10
(ppm)						
Cu	77	30	850	1.29	314	53
Pb	22	1.0	150	0.78	312	13
Zn	116	72	370	0.41	314	131
As	10	0.8	43	0.72	140	7.6
Sb	1.0	0.25	2.6	0.43	140	1.4
Se	1.0	0.25	4.6	0.81	140	0.88
Hg*	455	85	2420	1.18	57	130
Ba	1598	0.0	27000	1.76	314	914
Ag	0.73	0.0	4.0	1.14	60	n.a.
Mo	3.2	1.0	40	1.82	140	1.1
Co	18	12	31	0.20	314	23
Cr	66	35	110	11.6	314	62
F	750	548	931	0.13	60	n.a.
La	5.2	4.0	34	0.27	314	22
Nb	8.3	0.0	20	0.71	253	9.4
Ni	34	0.0	92	0.55	314	57
Rb	18	51	130	0.20	253	87
Y	21	15	28	0.14	254	22
Yb	1.8	0.9	2.5	0.18	314	2.1
Zr	117	58	180	0.20	254	144
Sr	96	130	1000	0.33	314	278

Notes: C.V. = coefficient of variation; *Hg expressed in ppb; n.d. = not determined; n.a. = not analyzed. Mean of sediment remote from mineralization also tabulated for comparison.
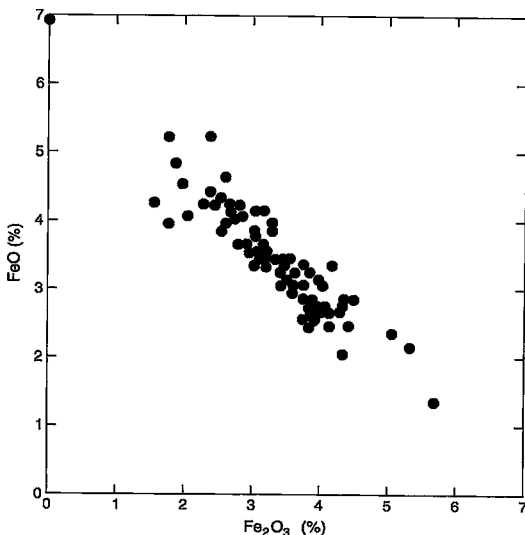

FIG. 15. Inverse correlation of FeO with Fe_2O_3 in unaltered hemipelagic sediment, Middle Valley.

and Sr, whereas Zone II is enriched in CaO, CO_2, Ba, Sr and, to a lesser extent, As, Se, Hg and Mo, compared to unaltered Holocene and latest Pleistocene sediment from Middle Valley. The bulk chemical composition of Zones I and II combined and of unaltered hemipelagic and turbiditic sediment is presented in Table 5. There is no apparent enrichment of Zn and Sb in altered hemipelagic sediment over unaltered hemipelagic sediment remote from known hydrothermal centers. The large range in CO_2, Zn and Sb values, together with major increases of these elements in Zone I, suggest that CO_2, Zn and Sb have been redistributed during hydrothermal alteration.

The stratigraphic zonation of elements in hydrothermally altered cores TUL89D–22 and TUL89D–17 from the AAV is shown in Figures 16 and 17, respectively. In core TUL89D–22, the sediment below about
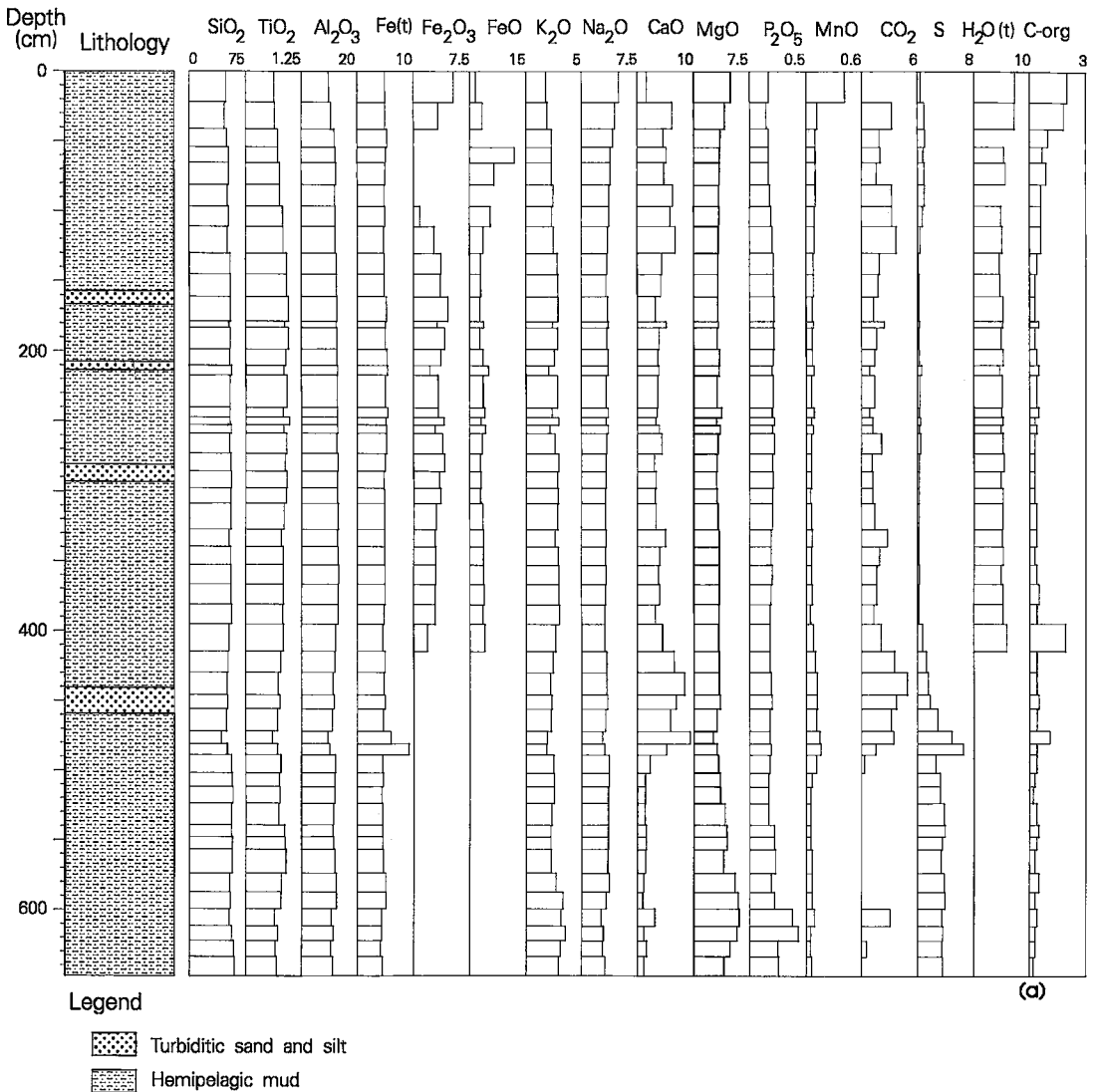
FIG. 16. Stratigraphic zonation of elements in core TUL88B–22, Area of Active Venting. (a) Major and minor elements; (b) minor and trace elements. Zone I: 480–645 cm; Zone II: 400–480 cm.

470 cm is moderately to strongly indurated, pale grey in color, enriched in MgO, P_2O_5, S, Zn, Cu, Pb, As, Sb, Se, and Ba, and depleted in CaO and CO_2 (Zone I). The transition between Zones I and II is marked by a sharp increase in CaO, CO_2, MnO, Sr, Cu, Pb, Zn, and Ba due to the deposition of sulfides, pyrite and carbonate at what is probably a chemical front separating the two zones. Some of the carbonate may be derived from biogenic carbonate that was leached from Zone I by outward and, perhaps, upward migrat-

ing hydrothermal fluids. Carbonate concretions are restricted to Zone II near the transition with Zone I.

The vertical zonation of elements in core TUL89D–17 is similar to core TUL89D–22 except that the magnitude of MgO enrichment in Zone I is greater. In core TUL87D–17, MgO approaches values of 12.5 wt.% at depths greater than 250 cm, whereas the carbonate content (*i.e.*, CO_2) approaches zero. In Zone I, the sediment is highly indurated, fractured, locally brecciated and cut by veins with narrow

(b)

Legend

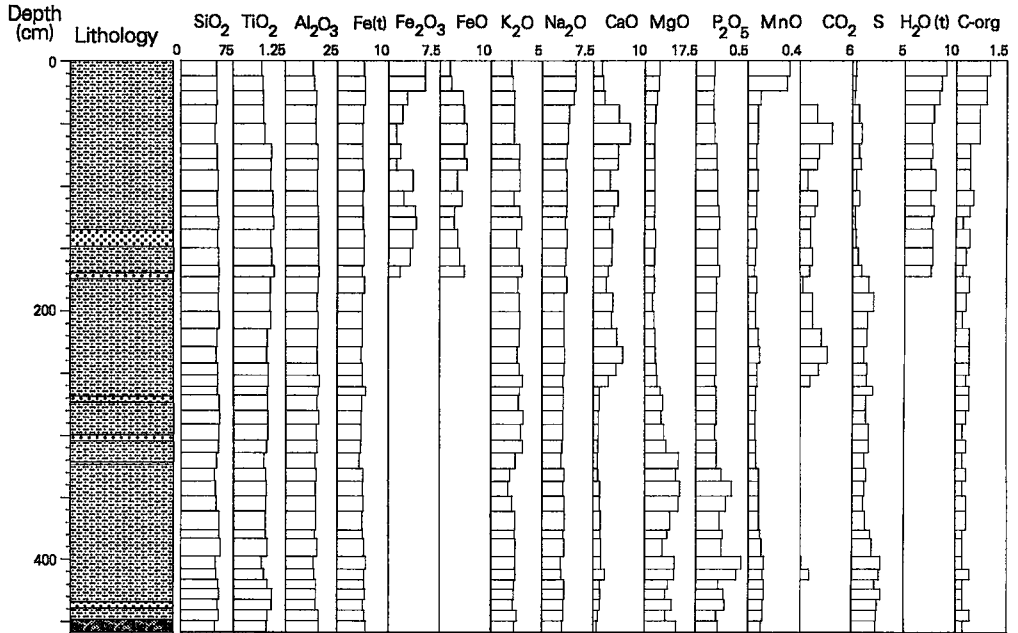   Turbiditic sand and silt

    Hemipelagic mud
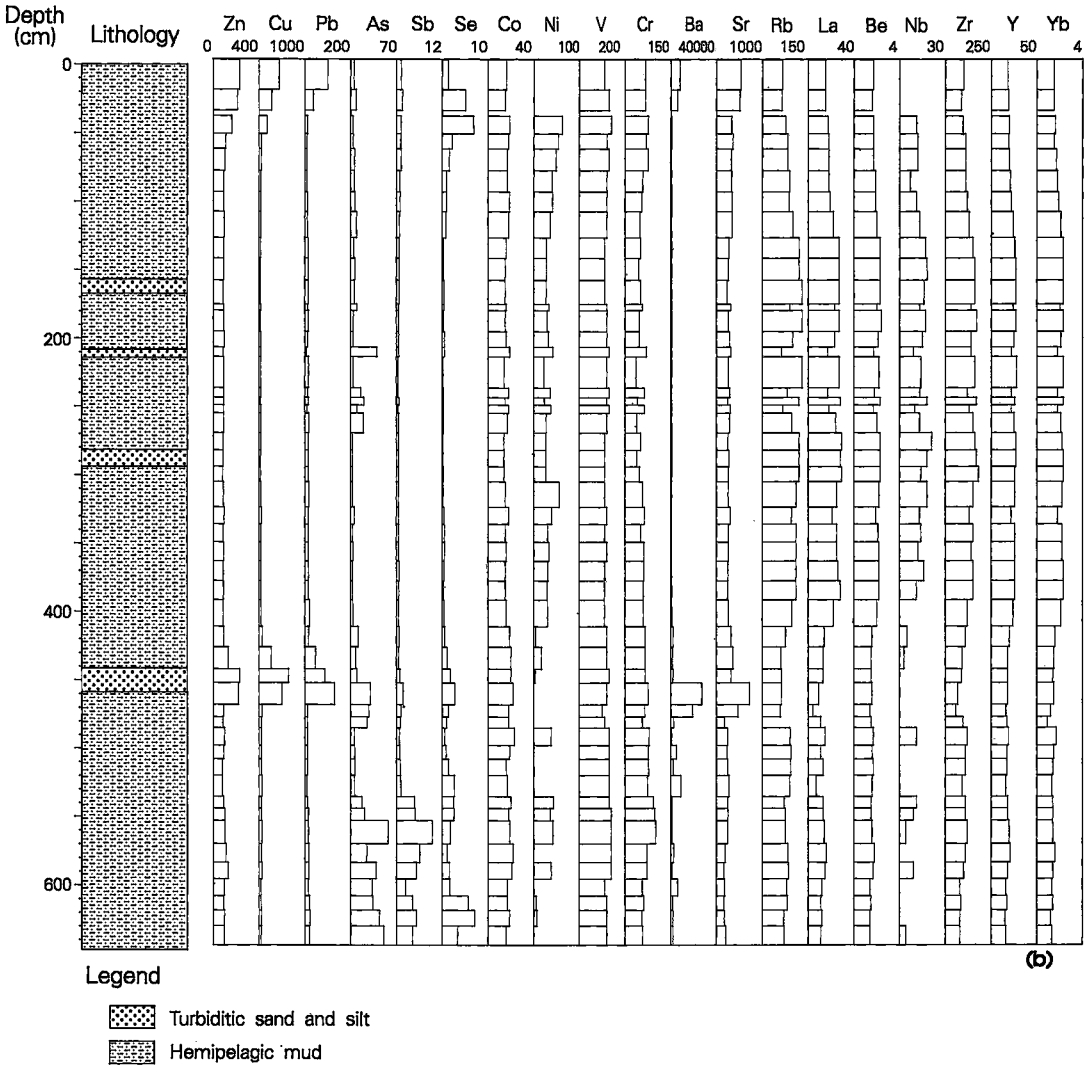
selvages of Mg-rich smectite-group minerals. Other elements enriched in Zone I include Mn, P, S, Zn, Cu, Pb, As, Sb, Se and Ba. There is a modest buildup of CaO and CO_2 near the upper margin of Zone I, similar to core TUL89D–22. The higher intensity of alteration in core TUL89D–17 compared to core TUL89D–22 is probably due to its closer proximity to vent sites.

The lateral zonation of MgO, S, Ba and CaO about active hydrothermal vent sites is illustrated with contours of average values for all samples analyzed in cores from AAV (Fig. 18). Sulfur (Fig. 18c) and MgO

(Fig. 18b) are concentrated over a broad area and generally increase toward active vents sites. Barium (Fig. 18d), however, is more proximally distributed around vent sites, whereas CaO (Fig. 18a) is depleted near the center of fluid discharge but is elevated near the inner margin of alteration Zone II. The lateral zonation of these elements is consistent with their stratigraphic distributions (Figs. 16, 17), which show marked depletions of carbonate carbon in the high-Mg, pyritic zone (Zone I) and a buildup of CO_2 near the base or most vent-proximal part of Zone II.

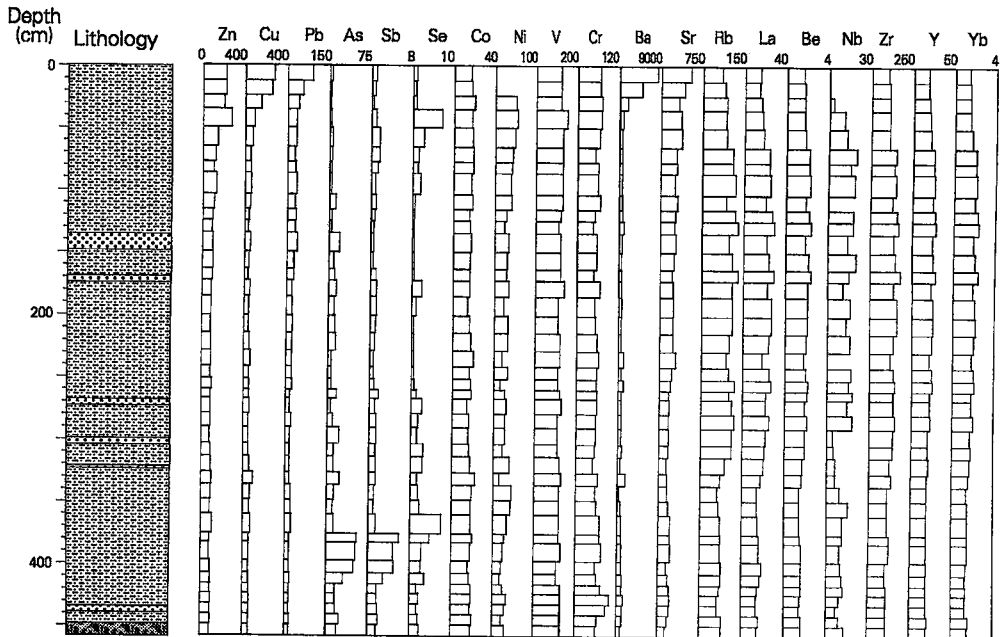## TUL89D-17

Major Elements (wt. %)

Legend   Hemipelagic mud   Mud-clast breccia   Turbiditic sand and silt   a)

TUL89D-17

Trace Elements (ppm)

Legend   Hemipelagic mud   Mud-clast breccia   Turbiditic sand and silt   b)
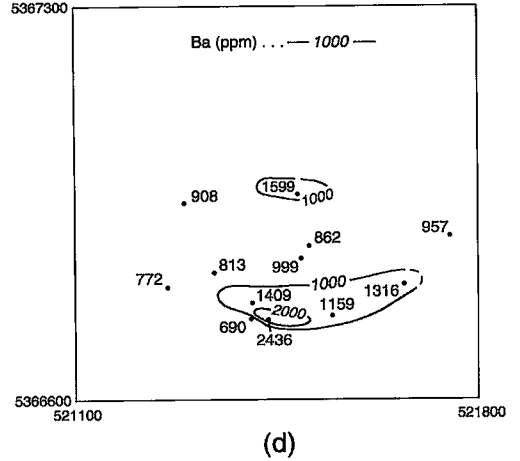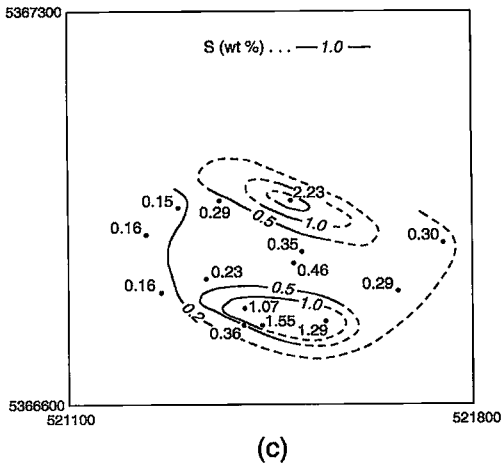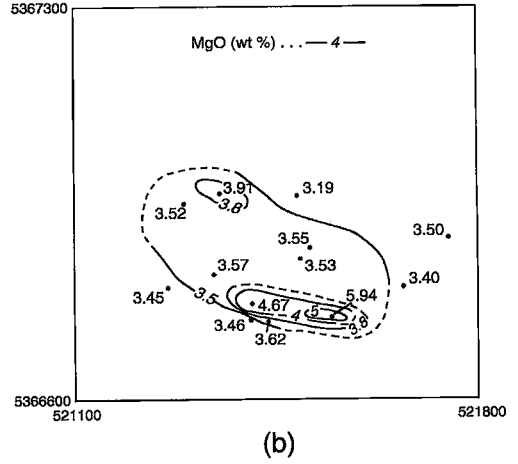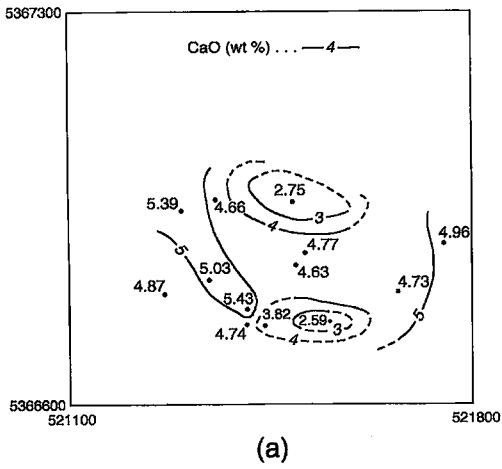
FIG. 18. Contours of the average contents of major elements in cores from the Area of Active Venting, Middle Valley; (a) CaO; (b) MgO; (c) S, and (d) Ba.
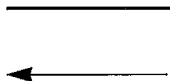
FIG. 17. Stratigraphic zonation of elements in core TUL89D–17, Area of Active Venting. (a) Major and minor elements; (b) minor and trace elements. Zone I: 260–460 cm; Zone II: 170–260 cm.

ISOTOPE GEOCHEMISTRY

Sulfur isotopes

Values of $\delta^{34}S$ for cubes of pyrite in hydrothermally altered hemipelagic sediment in cores TUL87B–11 and TUL87B–15 range between –21.1 and 10.6‰ (Table 6). Most values for pyrite, with the exception

of two samples near the bottom of core TUL87B–15, are positive and fall within the range of values for pyrite in the Bent Hill massive sulfide deposit (Goodfellow & Blaise 1988, Goodfellow & Franklin 1993). Values of $\delta^{34}S$ for acid-extractable pyrrhotite and sphalerite range between 5.4 and 10.4‰ and are generally more positive than those for pyrite. Pyritized worm burrows in core PAR85–34, however, are char-

TABLE 6. $\delta^{34}S$ VALUES FOR SULFIDES IN HYDROTHERMALLY ALTERED SEDIMENT, AAV

Sample Number	Description	$\delta^{34}S_{Po,Sp}(‰)$	$\delta^{34}S_{Py}(‰)$
TUL-87B-11			
01I	Altered H.P.S.	-	3.4
02I	Altered H.P.S.	7.5	2.7
03I	Altered H.P.S.	8.2	2.0
04I	Altered H.P.S.	8.1	7.2
05I	Altered H.P.S.	7.1	7.5
06I	Altered H.P.S.	7.9	2.4
07I	Altered H.P.S.	7.0	2.8
08I	Altered H.P.S.	9.8	3.8
09I	Altered H.P.S.	5.4	0.8
10I	Altered H.P.S.	10.4	4.7
12I	Altered H.P.S.	10.0	0.1
13I	Altered H.P.S.	7.1	5.5
TUL-87B-15			
01I	Hydrothermal Sediment	-	13.5
04I	Hydrothermal Sediment	-	11.7
05I	Altered H.P.S.	-	2.3
06I	Altered H.P.S.	-	10.6
07I	Altered H.P.S.	-	6.8
13I	Altered H.P.S.	-	-21.1
14I	Altered H.P.S.	-	-2.3
PAR85-34			
665-670cm	Pyritized worm tube		-19.4
370-372cm	Pyritized worm tube		-14.3
540-542cm	Pyritized worm tube		-38.5
548-550cm	Pyritized worm tube		-33.5
630-632cm	Pyritized worm tube		-12.4
340-342cm	Pyritized worm tube		-39.7

		$\delta^{34}S_{Brt}(‰)$
MV86		
DR01-12	Altered worm burrow	27.3
DR02-26	Altered H.P.S. with veins of silica/barite	33.6
DR01-27	Altered H.P.S. with barite in fractures and cavities	56.9
DR01-26	Altered H.P.S. with barite in fractures and cavities	45.7

		$\delta^{34}S_{Anh}(‰)$
MV86 DR01-01	Anhydrite crust	21.1
PAR85-43TR-01	Anydrite-rich sediment	21.9

Notes: H.P.S. = hemipelagic sediment

TABLE 7. STABLE ISOTOPE COMPOSITIONS OF HYDROTHERMAL BARITE, GYPSUM, SILICATES AND ALTERED AND UNALTERED HEMIPELAGIC SEDIMENT FROM MIDDLE VALLEY

	$\delta^{18}O$ SMOW	$\delta^{13}C$ PDB
Carbonate Concretion (AAV)		
PAR85-34-2 5-7cm	33.97	-38.18
PAR85-34-2 13-15cm	34.05	-35.30
PAR85-34-2 22-24cm	33.88	-33.07
PAR85-34-2 81-82cm	33.65	-31.44
PAR85-34-2 130-133cm	32.77	-34.26
PAR85-34-2 140.5-141.5cm	32.46	-32.65
PAR85-34-2 143-144cm	32.59	-35.37
PAR85-34-5 95-96cm	23.34	-15.27
PAR85-34-6 11-12.5cm	20.80	-14.96
PAR85-34-6 24-25cm	21.08	-15.78
PAR85-34-6 85.1-86.1cm	19.56	-14.80
PAR85-34-6 90-90.5cm	18.66	-14.45
PAR85-34-6 109-114cm	19.75	-19.25
PAR85-34-7 120-123.5cm	30.07	-23.39
TUL87B-15-8I	19.03	-25.11
TUL87B-15-9I	23.30	-27.49
TUL87B-15-10I	17.09	-22.13
Gypsum (BH and AAV)		
PAR85-13-43	9.8	
PAR85-34-900/902	6.0	
PAR85-34-920/922	4.7	
Barite (BH)		
PAR85-13-84-94	3.3	
PAR85-13-6-14	12.9	
PAR85-13-120-128	18.8	
PAR85-13-215-219	14.4	
PAR85-13-141.5-147	15.6	

	$\delta^{18}O(SMOW)$	$\delta D(SMOW)$
Saponite (AAV)		
PAR85-43	12.1	-72
TUL87B-15-1 30-45cm	12.5	-77
Talc (BH)		
PAR85-13	11.3	-69
PAR85-13-39C	18.9	-70
Altered Sediment(AAV)		
TUL87B-15-03 30-45cm	10.6	-83
TUL87B-15-03 128-131cm	10.6	-74
Unaltered Sediment		
PAR85-14 20-40cm	10.9	-63
PAR85-14 120-130cm	11.7	-86

Values quoted in ‰

acterized by negative $\delta^{34}S$ values between –12.4 and –38.5‰, and are similar to isotopically light black diagenetic sulfides, with $\delta^{34}S$ values between –10 and –40‰ (Goodfellow & Blaise 1988).

Barite veins cutting hydrothermally altered sediment are isotopically heavy, with $\delta^{34}S$ values that range between 27.3 and 56.9‰ (Table 6). These values are considerably more positive than barite from the BH massive sulfide deposit (average value of 10.1‰; Goodfellow & Blaise 1988) and anhydrite crust and sediment from the AAV, that have values similar to modern seawater (about 20.8‰).

Carbon, oxygen and hydrogen isotopes

Values of $\delta^{13}C$, $\delta^{18}O$ and δD for hydrothermal minerals from Middle Valley are presented in Table 7.

Values of $\delta^{13}C$ in calcite from carbonate concretions range between –14.45 and –38.18‰ (Table 7; Goodfellow & Blaise 1988) and are considerably more negative than values for Holocene foraminifers from Middle Valley, which range between –0.5 and +0.5‰ (Al-Assam & Bornhold 1986). Values of $\delta^{13}C$ and $\delta^{18}O$ increase and decrease with depth in core PAR-85–34, respectively (Fig. 19; Al-Assam & Blaise 1991).

Values of $\delta^{18}O$ for calcite in carbonate concretions range between 17.09 and 33.97‰ (Table 7). Calculated temperatures of precipitation using the fractionation factors of O'Neil *et al.* (1969), and assuming equilibrium conditions and a $\delta^{18}O_{H2O}$ of 0.0‰, range between 20°C to 120°C (Fig. 19). These temperatures are comparable to temperatures calculated for barite, which range between 65° and 114°C,
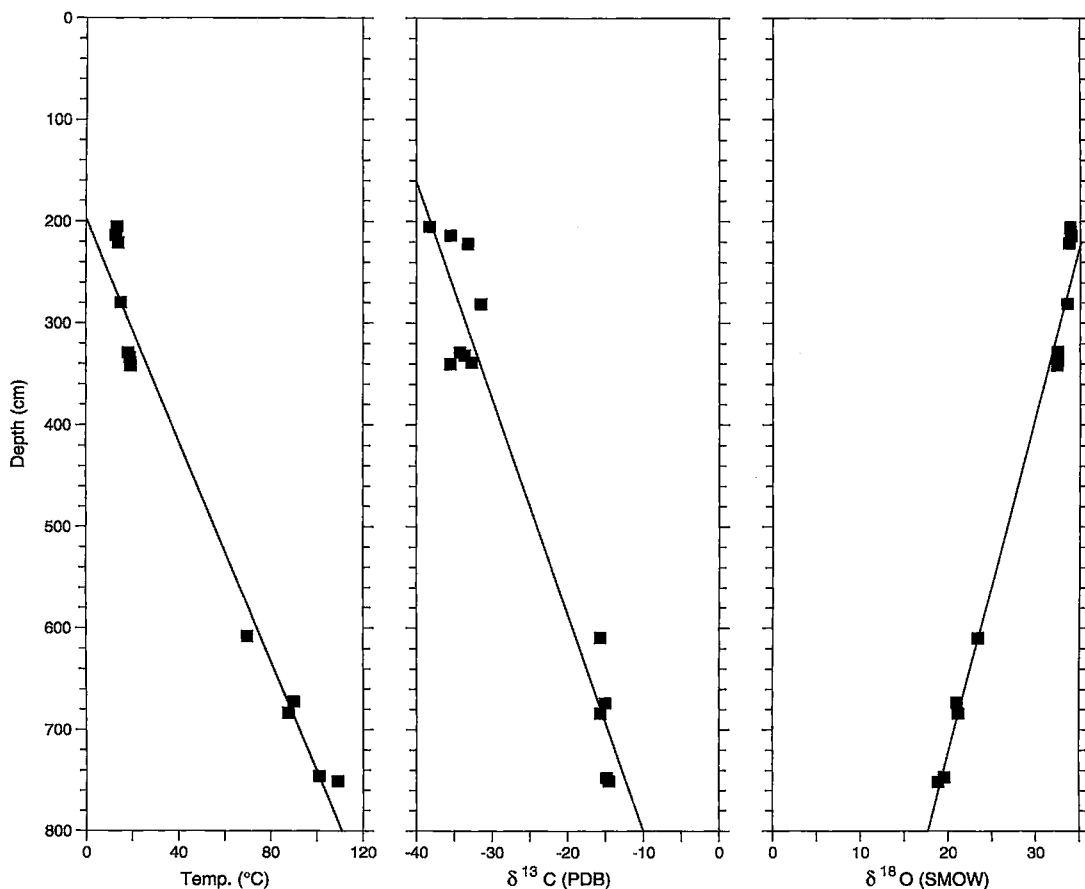

FIG. 19. Values of $\delta^{13}C$, $\delta^{18}O$ and temperature (°C) *versus* depth in core PAR 85–34, Area of Active Venting. Temperature was calculated using the fractionation equation of O'Neil *et al.* (1969) for calcite and H_2O, and assuming a $\delta^{18}O$ for H_2O of 0.0 ‰.
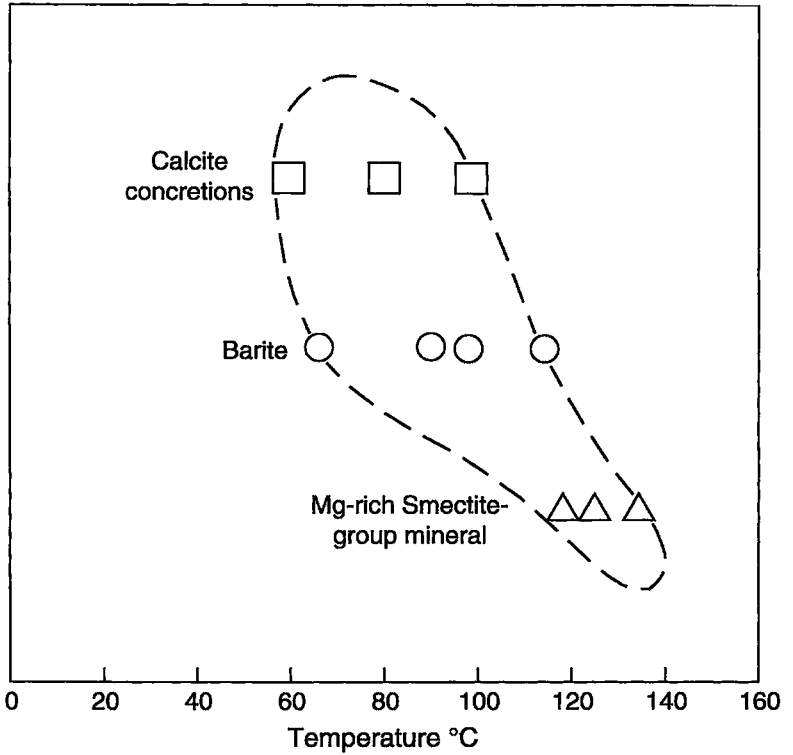
FIG. 20. Oxygen isotope fractionation temperatures calculated for hydrothermal minerals from Middle Valley. Fractionation factors are from the following sources: Calcite – H_2O (O'Neil et al. 1969); barite – H_2O (Kusakabe & Robinson 1977); smectite – H_2O (Yeh & Savin 1977). A $\delta^{18}O$ of 0.0 ‰ was used for H_2O, although this value probably varies as a function of mixing between end-member hydrothermal fluids, pore water and seawater.
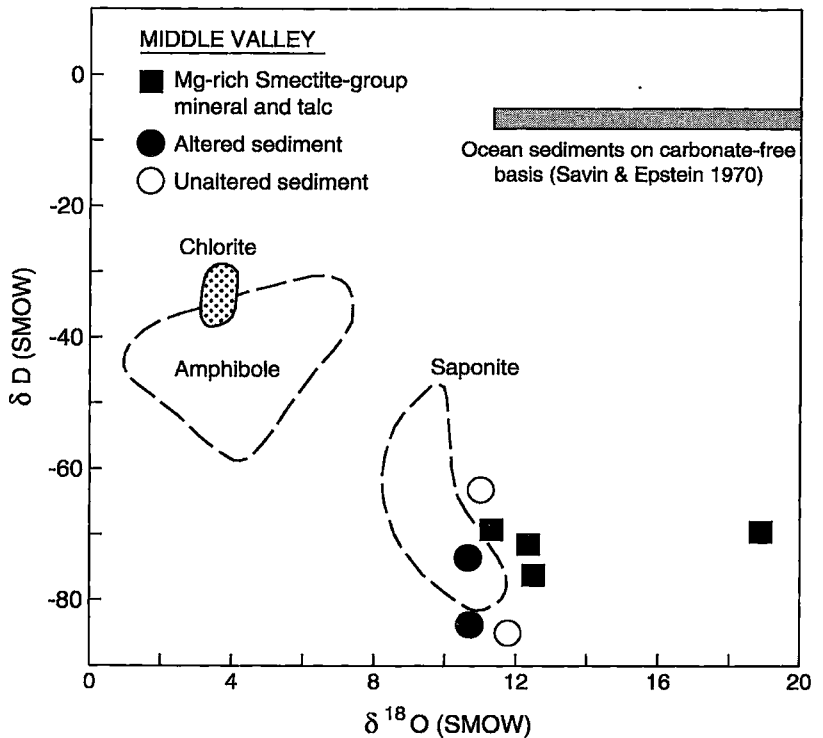

FIG. 21. Binary δD versus $\delta^{18}O$ plot for hydrothermal sediment and hydrothermally altered hemipelagic sediment from the Area of Active Venting, Middle Valley. Field of carbonate-free ocean sediment from Savin & Epstein (1970); saponite, chlorite and amphibole fields from Stakes & O'Neil (1982) and Stakes et al. (1984).

based on the equation for oxygen isotope fractionation between barite and H_2O (Kusakabe & Robinson 1977). Isotope-fractionation temperatures determined for hydrothermal Mg-rich smectite-group minerals (saponite) from BH and AAV define a narrow range (i.e., 119° to 134°C) and are greater than those calculated for carbonate and barite (Fig. 20). Calculated temperatures for hydrothermal minerals are consistent with the formation of saponite in Zone I near the center of high-temperature fluid discharge, and the formation of calcite in Zone II, further from the hydrothermal vents.

Values of δD are highly negative for both hydrothermally altered sediment and hydrothermal talc and Mg-rich smectite-group minerals in Middle Valley (Table 7, Fig. 21). Most samples plot near the field for saponite outlined by Stakes et al. (1984) and Stakes & O'Neil (1982). Values of $\delta^{18}O$ for hydrothermal talc and Mg-rich smectite-group minerals are consistently greater than values for hemipelagic sediment, whereas $\delta^{18}O$ values for hydrothermally altered sediment are less than those for unaltered sediment.

Strontium isotopes

Ratios of $^{87}Sr/^{86}Sr$ for hydrothermal minerals, and hydrothermally altered and unaltered hemipelagic sediment, are presented in Table 8. Hydrothermal

TABLE 8. INITIAL $^{87}Sr/^{86}Sr$ RATIO OF HYDROTHERMAL MINERALS, ALTERED AND UNALTERED SEDIMENTS, MIDDLE VALLEY

	$^{87}Sr/^{86}Sr$
Barite (BH)	
PAR85-13	0.70540
MV86DR01-12	0.70597
MV86DR02-26	0.70552
Calcite (AAV)	
TUL87B-15-8I	0.70617
TUL87B-15-9I	0.70694
TUL87B-15-10I	0.70671
Gypsum (BH)	
PAR85-13-42	0.70655
Hydrothermally Altered Sediment (AAV)	
TUL87B-15-01 30-45cm	0.70727
TUL87B-15-01 128-131cm	0.70828
Unaltered Sediment	
PAR85-14 20-40cm	0.70877
PAR85-14 120-130cm	0.71131

minerals have $^{87}Sr/^{86}Sr$ values that plot between those typical of recent MORB basalt (Ito et al. 1987, MacDougall & Lugmair 1986) and modern seawater (Brass 1976) or unaltered hemipelagic and turbiditic sediment from Middle Valley (Fig. 22). Values of $^{87}Sr/^{86}Sr$ for altered hemipelagic sediment are consistently lower than those for unaltered sediment (Table 8), and values for unaltered Middle Valley sediment partly overlap those typical of average continental crust (Faure et al. 1963) but are, on average, less radiogenic. The data indicate that calcite precipitated from a fluid that was more evolved, and therefore further from vent sites, than that from which barite formed. Gypsum and calcite have similar ratios, although $^{87}Sr/^{86}Sr$ ratios for gypsum were probably altered (increased) during the hydration of anhydrite by seawater.

DISCUSSION

Hydrothermal alteration in the AAV consists of an inner spatially restricted high-temperature zone (Zone I) that is surrounded by a more widespread lower-temperature outer zone (Zone II) (Fig. 5). Hemipelagic and turbiditic sediments hosting the BH sulfide deposit are altered to hydrothermal minerals similar to those in the AAV, but the alteration zones have been dismembered and displaced by resedimentation and slumping along the margins of mounds. Alteration zones plotted on two cross-sections of the AAV display a convex upward pattern (Figs. 6, 7). The domal shape is supported by other cross-sections and the distribution of Ba, Ca, SiO_2 and Mg in pore waters (Lydon et al. 1991). Within Zone I, the normally olive grey and tan grey hemipelagic sediment is highly indurated and pervasively altered to a pale grey color. Hydrothermal minerals include a Mg-rich smectite-group mineral (probably saponite), chlorite, silica, barite, euhedral pyrite and gypsum. These minerals form veins, infill open spaces in porous turbidites and silty clay, and replace hemipelagic and turbiditic sediment. Veins and open fractures that generally cut bedding planes at a high angle are more abundant in Zone I than in Zone II, and are more common near vents. Sediment that is cut by veins is commonly disrupted by brecciation and faulting. Most of the veins have narrow selvages, typically less than 2 cm wide, that consist of mostly Mg-rich smectite-group minerals. Zone I is generally depleted in carbonate relative to unaltered Holocene hemipelagic sediment, due to the dissolution of biogenic carbonates by hydrothermal fluids. Compared to unaltered hemipelagic sediment, Zone I is enriched in Mg, S, Ba, Cu, Pb, As, Sb, Se, Hg and Mo, and depleted in Ca, carbonate C and Sr.

Within Zone II, olive grey and tan grey hemipelagic sediments are weakly to moderately indurated and have a blue-green hue due to the dominance of
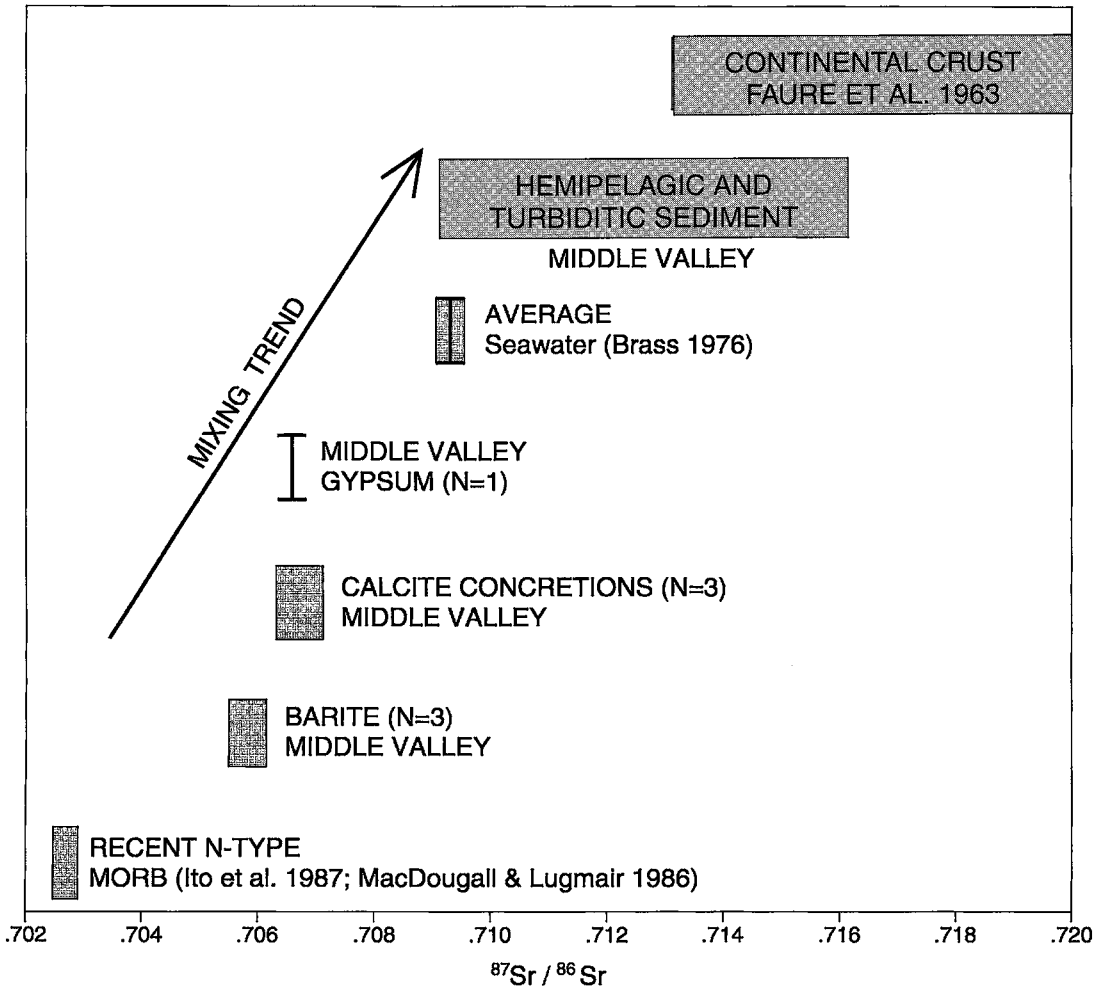
FIG. 22. Plot of $^{87}Sr/^{86}Sr$ ratios for hydrothermal calcite, barite, gypsum, and altered and unaltered hemipelagic and turbiditic sediment, Middle Valley. Also plotted for comparison are ratios for continental crust (Faure *et al.* 1963), recent N-type MORB basalts (Ito *et al.* 1987, MacDougall & Lugmair 1986) and average seawater (Brass 1976).

Mg-rich smectite-group minerals. The low content of Mg-rich smectite-group minerals in unaltered cores is consistent with a hydrothermal origin. Near the margins of Zone II, the alteration is not pervasive, but restricted to intervals of interbedded hemipelagic and turbiditic sediments that have a high along-strata permeability and are chemically reactive. Hydrothermal veins are uncommon in Zone II. In addition to a Mg-rich smectite-group phase, Zone II is composed of hydrothermal carbonate, barite, gypsum and minor pyrite. The carbonate occurs as concretions, replacements and infillings of worm burrows and foraminifers, and as cement in hemipelagic and turbiditic sediment. Euhedral pyrite commonly rims

carbonate concretions and carbonate-cemented worm burrows, and occurs disseminated throughout carbonate concretions. Zone II is enriched in Ca, carbonate C, Ba, Sr and, to a lesser degree, As, Se, Hg and Mo.

The high MgO and low CaO contents of Zone I (Fig. 23) reflect the presence of Mg-rich silicates and the dissolution of biogenic carbonate during reaction of hemipelagic sediment with hydrothermal fluid. High contents of pyrite S in altered sediment below a depth of 400 cm in core TUL89D–22 (Fig. 16), combined with uniform contents of total Fe, indicate that Fe in pyrite originated from the breakdown of Fe-bearing phases such as detrital magnetite, amphibole and chlorite. Elevated contents of most chalcophile ele-
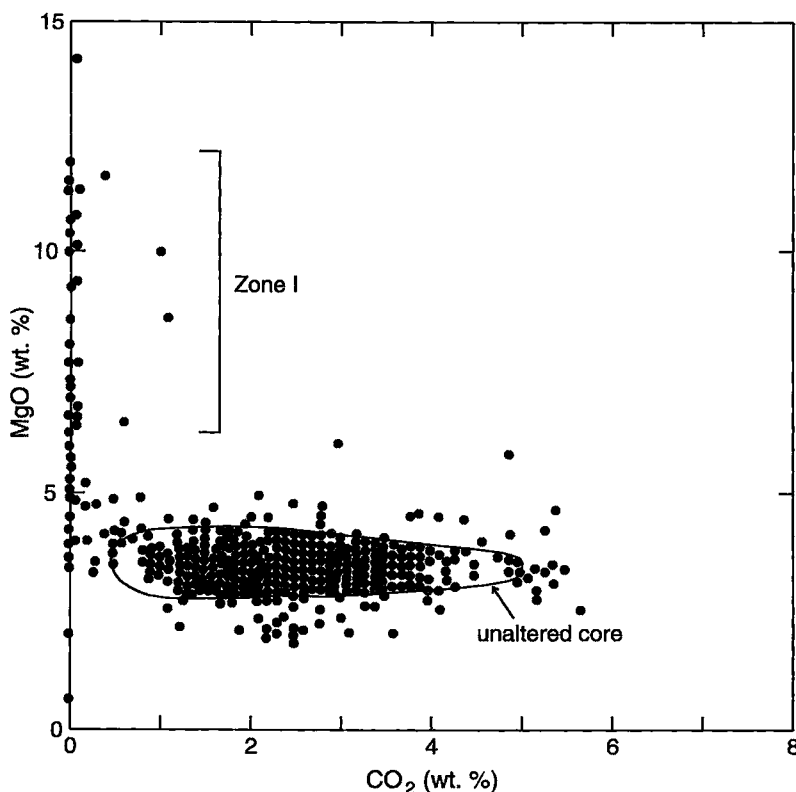
FIG. 23. Binary MgO–CO_2 plot of hydrothermally altered and unaltered hemipelagic and turbiditic sediment from the Area of Active Venting, Middle Valley. Samples with high MgO and very low CO_2 values correspond to alteration Zone I.

ments (*e.g.*, Cu, Pb, Zn, As, Sb, Se Hg and Mo) probably reflect trace amounts of chalcopyrite, sphalerite and possible other sulfides that were precipitated from hydrothermal fluids during alteration of the sediments. Barium, which is also elevated in Zone I, forms authigenic barite that precipitated by the mixing of hydrothermal Ba with seawater sulfate.

The zonal distribution of hydrothermal minerals in altered sediment surrounding active vents in the AAV reflects the chemical and physical evolution of a high-temperature hydrothermal fluid ($\sim$274°C) as it migrated upward and outward from a central conduit and mixed with pore water and downwelling seawater, and reacted with hemipelagic and turbiditic sediment. The precipitation of Mg-rich smectite-group minerals in Zones I and II can most readily be explained by the mixing of hydrothermal silica with seawater or porewater Mg. The model of a hydrothermal fluid that migrates upward and outward from a central vent is consistent with the compositions of pore water in the

sediment cores from the AAV. These fluids display strong vertical compositional gradients that define the margins of a convex-upward hydrothermal plume, with lateral dimensions that are similar to those of the AAV vent field (Lydon *et al.* 1991). Fluids from the center of the hydrothermal plume plot on a mixing line between AAV end-member hydrothermal fluids and seawater, and are concentrated in Ca (57 nM), Ba (5 nM) and Si and depleted in Mg (30 nM) and SO_4^{2-} (Lydon *et al.* 1992) relative to seawater (Von Damm 1990). Hemipelagic sediment from Zone II has been subjected to mild hydrothermal conditions (50–100°C), based on their bitumen composition (Simoneit *et al.* 1992). These temperatures fall within the temperature range for carbonate concretions calculated according to the fractionation of oxygen isotopes. The dissolution of biogenic carbonate minerals from Zone I is consistent with the reaction of hydrothermal fluids with unaltered hemipelagic sediment near vent sites. Temperatures of isotopic fractionation

for Mg-rich smectite-group minerals indicate that biogenic carbonates were dissolved at temperatures greater than 120°C. Calculated temperatures for hydrothermal calcite suggest that calcite precipitated at lower temperatures (<100°C) within Zone II. Carbonate concretions from core PAR85–34 have been dated at 20,090 ± 170, 19,410 ± 130 and 24,010 ± 180 aBP by the ^{14}C dating method. These dates are comparable to the age of foraminifers (21,010 ± 280 aBP) at a depth of 847–848 cm in core PAR85–34 and to the age of high-temperature bitumen (>300°C) in a barite chimney from AAV, that has a ^{14}C age of 29,000 aBP (Simoneit *et al.* 1992). The young ages indicate rapid recycling of the carbon at shallow depths within the sedimentary pile.

Other evidence for a hydrothermal fluid that evolved as it moved outward from the center of hydrothermal fluid discharge is provided by Sr and O isotopes. A decrease of δ^{18}O values for hydrothermally altered sediment indicates that major exchange of oxygen has taken place between hemipelagic sediment and hydrothermal fluid (Fig. 21). Strontium isotope values of hydrothermal barite, carbonate and gypsum from the AAV show that isotopically primitive Sr, probably of basaltic origin, was modified by mixing with more radiogenic Sr (Fig. 22). There are two possible sources of radiogenic Sr, seawater or the sedimentary pile. In the latter case, the Sr would have been leached from biogenic or detrital minerals at depth within the zone of hydrothermal reaction, or at shallower depths within the upflow zone. A consistent trend of increasing ^{87}Sr/^{86}Sr ratios with increasing distance from active vents suggests that laterally migrating hydrothermal fluids reacted with sediment or mixed with pore water and seawater in the near-seafloor (<10 m depth) environment.

The transition between Zones I and II is characterized by a buildup of hydrothermal carbonate concretions, cement and lesser veins. Within Zone II, the concretions occur within discrete intervals of hemipelagic sediment, commonly near contacts with interbedded silty and sandy turbidites. This nonuniform distribution suggests that concretions formed either by the lateral migration of hydrothermal fluids along more permeable horizons, or at different times in the history of hydrothermal activity in the area, or both. The lack of chemical or mineralogical differences between hemipelagic sediment that hosts concretions and sediment barren of concretions negates a compositional control on the distribution of concretions. The occurrence of carbonate concretions at the boundary between oxidized, brown surface mud and less oxidized olive grey mud in core TUL88B–22 suggests that the oxidation of hydrothermal methane by sulfate-reducing bacteria may have increased the activity of dissolved carbonate and promoted the precipitation of carbonate. The principal reaction proposed by Reeburgh (1980) to regulate the distribution

of sulfate and methane in marine sediments is:

$$CH_4 + SO_4^{2-} = HS^- + HCO_3^- + H_2O.$$
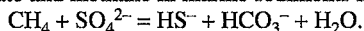
Values of δ^{13}C for carbonate concretions are consistently more negative (Table 7) than values for foraminifers (Al-Assam & Bornhold 1986) and within the range of values for CO_2 from the vent fluid (Taylor 1990). Vent fluids at Middle Valley are enriched in dissolved carbonate (CO_2) and methane in "apparent equilibrium" with δ^{13}C values between –32.98 and –10.64‰, and between –61.53 and –52.19‰, respectively (Taylor 1990). Highly negative values of δ^{13}C for carbonate concretions suggest that most of the carbon in these concretions originated from the oxidation of organic compounds such as methane, either thermogenically within the sedimentary pile or biogenically near the seafloor. If hydrothermal calcite precipitated from a chemically uniform end-member hydrothermal fluid under equilibrium conditions, however, δ^{13}C and δ^{18}O values for calcite would be expected to correlate positively as a function of temperature (Fig. 24) or fall on a mixing line between hydrothermal and seawater carbonate. Instead, measured δ^{13}C and δ^{18}O values for hydrothermal calcite in core PAR 85–34 staddle the 100°C isotherm due to changes in initial values. The positive correlation of δ^{13}C with temperature (Fig. 19) shows that the contribution of isotopically light carbon is greater in Zone II, away from hydrothermal vents. This suggests that hydrothermal methane was oxidized to carbonate in the outer and lower-temperature part of the zone of upflow of hydrothermal fluid. The common association of euhedral pyrite with hydrothermal carbonate indicates that sulfate was probably reduced by methanogenic bacteria at temperatures less than 100°C

Additional evidence for carbon oxidation during hydrothermal alteration is provided by the sulfur isotope composition of pyritized carbonate-cemented worm burrows and barite in altered sediment. Values of δ^{34}S for hydrothermal barite that are more positive than contemporaneous seawater indicate that the sulfur isotopes have been fractionated by bacterial reduction under closed or partly closed conditions within the zone of upflow of hydrothermal fluid. The low temperatures of barite and carbonate formation (<120°C; Fig. 20) make it highly unlikely that inorganic sulfate reduction and coupled organic carbon oxidation have occurred during the hydrothermal alteration of sediment. Experimental studies by Kiyosu (1980) have shown that sulfate is reduced to sulfide by reaction with organic matter at temperatures above 250°C. Highly negative values of δ^{34}S (–19.4 to –38.5‰; Table 6) for pyrite in carbonate-cemented worm burrows demonstrate that the bacterial reduction of sulfate has probably increased values for residual pore-water sulfate. These sulfur isotope values contrast markedly with δ^{34}S values for the euhedral pyrite from Zone I, which are more positive and within the
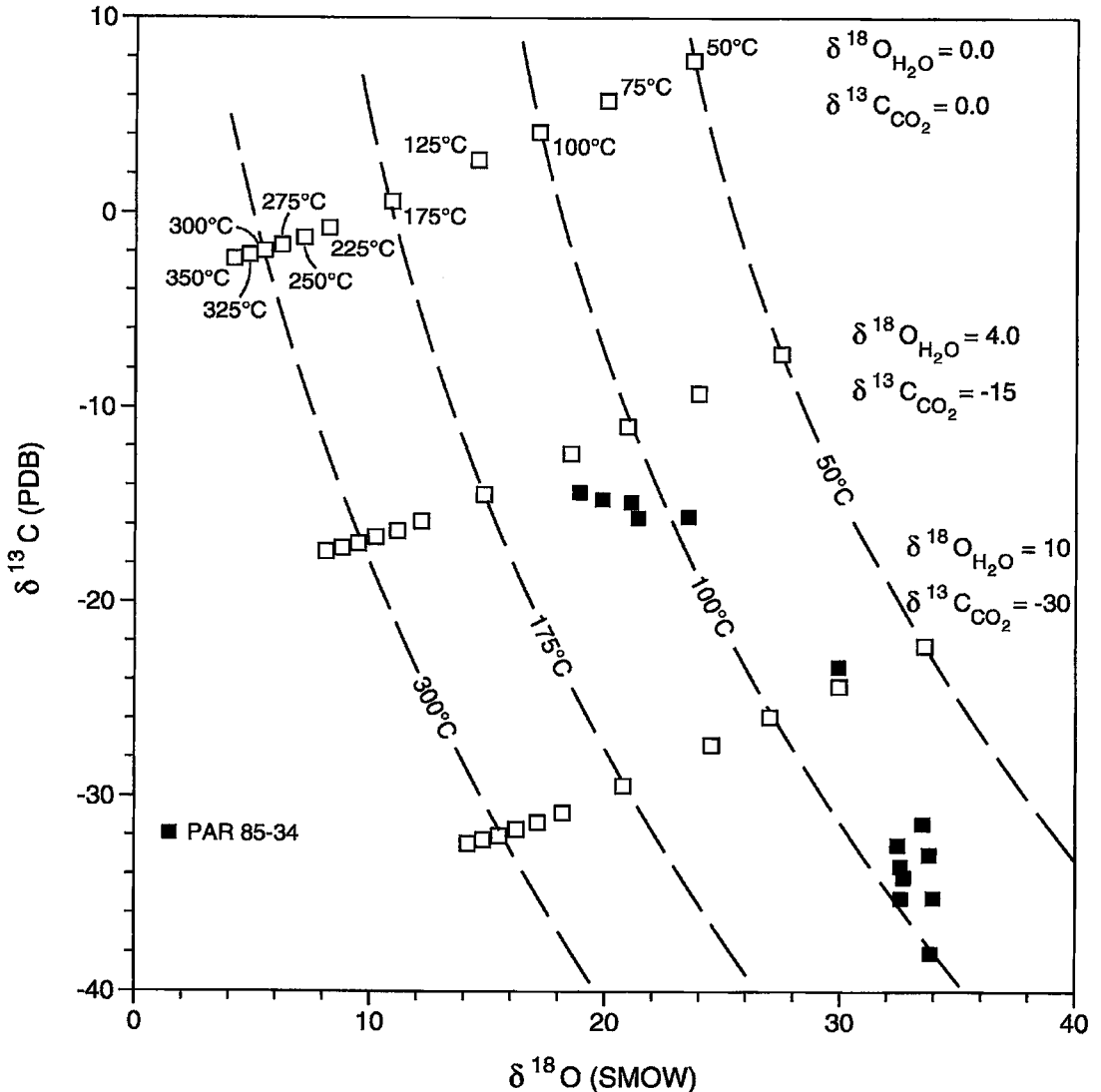
FIG. 24. Equilibrium values of $\delta^{13}C$ and $\delta^{18}O$ for calcite that precipitated from fluids with different $\delta^{13}C_{CO2}$ and $\delta^{18}O_{H2O}$ over the temperature range 50° to 350°C. Equilibrium fractionation factors are from the following sources: oxygen isotope fractionation between calcite and H_2O (O'Neil *et al.* 1969); carbon isotope fractionation between calcite and CO_2 (Bottinga 1969).

range of values for the BH sulfides.

The local hydrology (in shallow conduits) is probably very complex owing to low cross-stratal permeability within the sedimentary sequence, capping of the upflow zone by hydrothermal minerals, and throttling of vents by precipitating hydrothermal minerals in fluid conduits. The restriction of altered sediment in Zone II to hemipelagic sediment interbedded with more permeable turbiditic units provides evidence of

lateral flow. The precipitation of carbonate interstitially within hemipelagic and turbiditic sediment may have capped the zone of hydrothermal discharge and promoted the lateral flow of hydrothermal fluids. In Zone I, however, the hemipelagic sediment is more indurated and has undergone brittle deformation. Fractures, some filled with hydrothermal minerals, and breccias cutting indurated sediment show that the cross-strata permeability was locally high, particularly
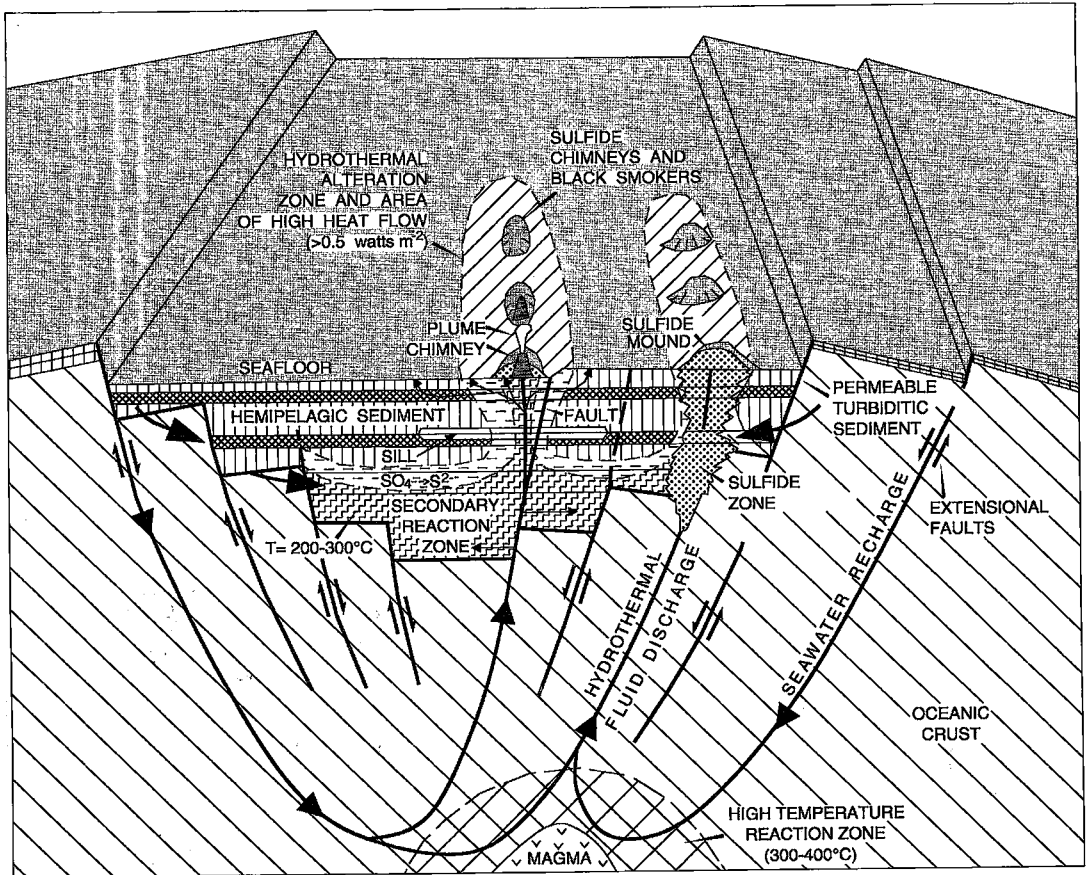
FIG. 25. Hydrothermal model of the Middle Valley sedimented rift showing the distribution of known sulfide deposits, hydrothermal alteration of sediments in zones of fluid upflow, possible patterns of hydrothermal fluid circulation, a hydrothermal "secondary" reaction zone at the base of the sedimentary pile, and inferred sulfides in the underlying sedimentary sequence at Bent Hill (from Goodfellow & Franklin 1993).

in the indurated core of the upflow zone. An increase in the confining pressure resulting from the capping and throttling of the hydrothermal system would force hydrothermal fluids to migrate laterally (Fig. 25). During periods of unrestricted discharge of fluids, however, seawater would probably be entrained into the discharge conduit, resulting in the dumping of Mg in the form of Mg-rich silicates. Since the sealing and breaching of the upflow zone most likely occur episodically, lateral migration of hydrothermal fluids and the entrainment of seawater are probably temporally variable. Added to these factors are changes to the physical properties of the sediment during hydrothermal alteration. Highly indurated hemipelagic sediments are susceptible to hydrofracturing, which increases the permeability in the high-temperature core of fluid-discharge conduits, whereas the sur-rounding weakly altered sediments deform plastically. As a result, the cross-stratal permeability is high in the core of the upflow zone, but low in adjacent weakly altered sediments. The effect of this contrasting permeability on fluid flow is to force hydrothermal fluids to migrate laterally along more permeable layers (e.g., turbiditic silt and sand beds) where upward flow of fluid in the core is throttled owing to the sealing or constriction of conduits by mineral precipitation.

CONCLUSIONS

1. The AAV vent field hosts at least 15 vent sites that are actively discharging hydrothermal fluids up to 274°C from anhydrite chimneys situated on sediment mounds. The BH area consists of one inactive and two hydrothermally active sulfide mounds.

2. Hemipelagic and turbiditic sediments near vent sites at AAV and BH are moderately to intensely indurated, locally brecciated, fractured and veined, and variably altered to hydrothermal silicates, carbonate, sulfates and sulfides.

3. At the AAV, the hydrothermal alteration consists of an inner, spatially restricted zone (Zone I) that consists of Mg-rich smectite-group minerals, chlorite, amorphous silica, barite, cubic pyrite and gypsum. Zone I is surrounded by hemipelagic and turbiditic sediment altered to Mg-rich smectite-group mineral, carbonate, barite and minor pyrite (Zone II).

4. Compared to unaltered hemipelagic sediment, Zone I is enriched in Mg, S, Ba, Cu, Pb, As, Sb, Se, Hg and Mo, and depleted in Ca, carbonate C and Sr; Zone II is enriched in Ca, carbonate C, Ba, Sr and, to a lesser degree, As, Se, Hg and Mo.

5. Temperatures based on isotopic fractionation for Mg-rich smectite-group minerals, barite and calcite indicate that Zone-I minerals formed at temperatures greater than 120°C, whereas Zone-II minerals formed at temperatures less than 100°C.

6. Values of $\delta^{13}C$ for carbonate concretions are consistently more negative than values for foraminifers and within the range of values for vent fluid CO_2. The large range of $\delta^{13}C$ values for carbonate carbon and the decrease of these values away from vents suggest that a major component of this carbonate carbon formed by the bacterial oxidation of hydrothermal methane. Ages of the carbonate concretions based on ^{14}C (20,090 ± 170, 19,410 ± 130 and 24,010 ± 180 aBP) that are comparable to the age of foraminifers (21,010 ± 280 aBP) at a depth of 847–848 cm indicate rapid recycling of the carbon at shallow depths within the sedimentary pile.

7. Strongly negative $\delta^{34}S$ values (−19.4 to −38.5‰) for pyrite in carbonate-cemented worm burrows indicate that sulfate was probably reduced by bacteria that utilized hydrothermal methane. Values of $\delta^{34}S$ for barite that are more positive than contemporaneous seawater likewise indicate that the sulfur isotopes have been fractionated by reduction of bacterial sulfate under closed or partly closed conditions. These sulfur isotope values contrast markedly with $\delta^{34}S$ values for pyrite cubes from Zone I, which are more strongly positive and within the range of values for the hydrothermal BH sulfides.

8. Sr isotope ratios of hydrothermal barite, carbonate and gypsum from the AAV define a mixing line, from more primitive Sr of basaltic origin near vents to more radiogenic Sr of seawater or sediment origin on the margins of the upflow zone.

9. The zonal distribution of hydrothermal minerals is controlled by the chemical and physical evolution of high-temperature (up to 274°C) fluid as it migrated outward and upward from a central conduit, reacted with detrital and biogenic minerals, and mixed with downwelling seawater.

REFERENCES

AL-ASSAM, A.I. & BLAISE, B. (1991): Interaction between hemipelagic sediment and hydrothermal system: Middle Valley, northern Juan de Fuca Ridge, subarctic Northeast Pacific. *Mar. Geol.* **98**, 25-40.

———— & BORNHOLD, B.B. (1986): Stable isotope studies of planktonic foraminifera *Globigerina bulloides* from cores in the NE Pacific Ocean. *Geol. Surv. Can., Pap.* **86-1B**, 201-212.

BOTTINGA, Y. (1969): Calculated fractionation factors for carbon and hydrogen isotopic exchange in the system calcite – carbon dioxide – graphite, methane – hydrogen – water vapor. *Geochim. Cosmochim. Acta* **33**, 49-64.

BRASS, G.W. (1976): The variation of the marine $^{87}Sr/^{86}Sr$ ratio during Phanerozoic time: interpretation using a flux model. *Geochim. Cosmochim. Acta* **40**, 721-730.

CHAMLEY, H. (1971): Recherches sur la sédimentation argileuse en Méditerranée. *Sci. Géol., Strasbourg, Mém.* **35**.

DAVIS, E.E., GOODFELLOW, W.D., BORNHOLD, B.D., ADSHEAD, J., BLAISE, B., VILLINGER, H. & LECHEMINANT, G.M. (1987): Massive sulfides in a sedimented rift valley, northern Juan de Fuca Ridge. *Earth Planet. Sci. Lett.* **82**, 49-61.

———— & SAWYER, B. (1987): Marine geophysical maps of western Canada. *Geol. Surv. Can., Bathymetric Map* **6-1987**.

———— & VILLINGER, H. (1992): Tectonic and thermal structure of the Middle valley sedimented rift, northern Juan de Fuca Ridge. *Proc. ODP (Ocean Drilling Program), Init. Rep.* **139**, 9-41.

FAURE, G., HURLEY, P.M. & FAIRBAIRN, H.W. (1963): An estimate of the isotopic composition of strontium in rocks of the Precambrian Shield of North America. *J. Geophys. Res.* **68**, 2323-2329.

FRANKLIN, J.M. AND THE LEG 139 SCIENTIFIC PARTY (1992): Formation of massive sulphide deposits in Middle Valley,

northern Juan de Fuca Ridge. *Geol. Surv. Can., Minerals Colloquium (Ottawa), Program Abstr.*, 20.

GOODFELLOW, W.D. & BLAISE, B. (1988): Sulfide formation and hydrothermal alteration of hemipelagic sediment in Middle Valley, northern Juan de Fuca Ridge. *Can. Mineral.* **26**, 675-696.

———— & FRANKLIN, J.M. (1993): Geology, mineralogy and geochemistry of massive sulfides in shallow cores, Middle Valley, Northern Juan de Fuca Ridge. *Econ. Geol.* **88** (in press).

HOLTZAPFFEL, T. (1985): Les minéraux argileux: préparation, analyse diffractométrique et détermination. *Ann. Soc. Géol. Nord, Publ.* **12**.

ITO, E., WHITE, W.M. & GÖPEL, C. (1987): The O, Sr, Nd and Pb isotope geochemistry of MORB. *Chem. Geol.* **62**, 157-176.

KIYOSU, Y., 1980. Chemical reduction and sulfur-isotope effects of sulfate by organic matter under hydrothermal conditions. *Chem. Geol.* **30**, 47-56.

KUSAKABE, M. & ROBINSON, B.W. (1977): Oxygen and sulfur isotope equilibria in the $BaSO_4$–HSO_4–H_2O system from 110 to 350°C and applications. *Geochim. Cosmochim. Acta* **41**, 1033-1040.

LYDON, J.W., GOODFELLOW, W.D. & FRANKLIN, J.M. (1991): Spatial control and pore water compositions of active and extinct hydrothermal fields in Middle Valley. *In* Int. Conf. on Fluids in Subduction Zones (Paris), Program Abstr. (J.-P. Cadet & X. Le Pichon, eds.).

————, ———— & GRÉGOIRE, D.C. (1992): Chemical composition of vent and pore fluids in an active hydrothermal discharge zone, Middle Valley. *Geol. Surv. Can., Minerals Colloquium (Ottawa), Program Abstr.*, 24.

MACDOUGALL, J.D. & LUGMAIR, G.W. (1986): Sr and Nd isotopes in basalts from the East Pacific Rise: significance for mantle heterogeneity. *Earth Planet. Sci. Lett.* **77**, 273-284.

O'NEIL, J.R., CLAYTON, R.N. & MAYEDA, T.K. (1969): Oxygen isotope fractionation in divalent metal carbonates. *J. Chem. Phys.* **51**, 5547-5558.

REEBURGH, W.S. (1980): Anaerobic methane oxidation: rate – depth distribution in Skan Bay sediments. *Earth Planet. Sci. Lett.* **47**, 345-352.

REES, C.E. (1978): Sulfur isotope measurements using SO_2 and SF_6. *Geochim. Cosmochim. Acta* **42**, 383-389.

SAVIN, S.M. & EPSTEIN, S. (1970): The oxygen and hydrogen isotope geochemistry of ocean sediments and shales. *Geochim. Cosmochim. Acta* **34**, 43-63.

SIMONEIT, B.R.T., GOODFELLOW, W.D. & FRANKLIN, J.M. (1992): Hydrothermal petroleum at the seafloor and organic matter alteration in sediments of Middle Valley, northern Juan de Fuca Ridge. *Appl. Geochem.* **7**, 257-264.

SPIVACK, A.J., PALMER, M.R. & EDMOND, J.M. (1987): The sedimentary cycle of the boron isotopes. *Geochim. Cosmochim. Acta* **51**, 1939-1949.

STAKES, D.S. & O'NEIL, J.R. (1982): Mineralogy and stable isotope chemistry of hydrothermally altered oceanic rocks. *Earth Planet. Sci. Lett.* **57**, 285-304.

————, TAYLOR, H.P., JR. & FISHER, R.L. (1984): Oxygen isotope and geochemical characterization of hydrothermal alteration in ophiolite complexes and modern ocean crust. *In* Ophiolites and the Oceanic Lithosphere (I.G. Gass, S.J. Lippard & A.W. Shelton, eds.). Blackwell Scientific Publications, Oxford, England (199-214).

TAYLOR, B.E. (1990): Carbon dioxide and methane in hydrothermal vent fluids from Middle Valley, a sediment-covered ridge segment. *Trans. Am. Geophys. Union (Eos)* **71**, 1569 (abstr.).

TURNER, R.J.W., LEITCH, C.H.B., AMES, D.E., HÖY, T., FRANKLIN, J.M. & GOODFELLOW, W.D. (1991): Character of hydrothermal mounds and adjacent sediments, active hydrothermal areas, Middle Valley sedimented rift, northern Juan de Fuca Ridge, northeastern Pacific: evidence from ALVIN push cores. *Geol. Surv. Can., Pap.* **91-1E**, 99-108.

VON DAMM, K.L. (1990): Seafloor hydrothermal activity: black smoker chemistry and chimneys. *Annu. Rev. Earth Planet. Sci.* **18**, 173-204.

YEH, HSUEH-WEN & SAVIN, S.M. (1977): Mechanism of burial metamorphism of argillaceous sediments. 3. O-isotope evidence. *Geol. Soc. Am. Bull.* **88**, 1321-1330.